An interdomain binding site on HIV-1 Nef interacts with PACS-1 and PACS-2 on endosomes to down-regulate MHC-I

Jimmy D. Dikeakos[a,*], Laurel Thomas[a,†], Grace Kwon[a], Johannes Elferich[b], Ujwal Shinde[b], and Gary Thomas[a,†]

[a]Vollum Institute and [b]Department of Biochemistry and Molecular Biology, Oregon Health and Science University, Portland, OR 97239

ABSTRACT The human immunodeficiency virus type 1 (HIV-1) accessory protein Nef directs virus escape from immune surveillance by subverting host cell intracellular signaling and membrane traffic to down-regulate cell-surface major histocompatibility complex class I (MHC-I). The interaction of Nef with the sorting proteins PACS-1 and PACS-2 mediates key signaling and trafficking steps required for Nef-mediated MHC-I down-regulation. Little is known, however, about the molecular basis underlying the Nef–PACS interaction. Here we identify the sites on Nef and the PACS proteins required for their interaction and describe the consequences of disrupting this interaction for Nef action. A previously unidentified cargo subsite on PACS-1 and PACS-2 interacted with a bipartite site on Nef formed by the $EEEE_{65}$ acidic cluster on the N-terminal domain and W_{113} in the core domain. Mutation of these sites prevented the interaction between Nef and the PACS proteins on Rab5 (PACS-2 and PACS-1)- or Rab7 (PACS-1)-positive endosomes as determined by bimolecular fluorescence complementation and caused a Nef mutant defective in PACS binding to localize to distorted endosomal compartments. Consequently, disruption of the Nef–PACS interaction repressed Nef-induced MHC-I down-regulation in peripheral blood mononuclear cells. Our results provide insight into the molecular basis of Nef action and suggest new strategies to combat HIV-1.

Monitoring Editor
Jean E. Gruenberg
University of Geneva

Received: Nov 18, 2011
Revised: Mar 7, 2012
Accepted: Apr 6, 2012

This article was published online ahead of print in MBoC in Press (http://www.molbiolcell.org/cgi/doi/10.1091/mbc.E11-11-0928) on April 11, 2012.

Present addresses: *Department of Microbiology and Immunology, Schulich School of Medicine and Dentistry, University of Western Ontario, London, ON N6A 5C1, Canada; †Department of Microbiology and Molecular Genetics, University of Pittsburgh, School of Medicine, Pittsburgh, PA 15219.

Address correspondence to: Gary Thomas (thomasg@ohsu.edu or thomasg@pitt.edu).

Abbreviations used: 3AT, 3-aminotriazole; ARR, atrophin-1–related region; BiFC, bimolecular fluorescence complementation; CD, circular dichroism; CTL, cytotoxic T lymphocyte; CTR, C-terminal region; DAPI, 4′,6-diamidino-2-phenylindole; FBR, furin-binding region; FBS, fetal bovine serum; furin-DD, furin containing $S_{773}S_{775}$→DD phosphomimetic mutations; GST, glutathione *S*-transferase; HA, hemagglutinin; His_6, hexahistidine; HIV-1, human immunodeficiency virus type 1; mAb, monoclonal antibody; MHC-I, major histocompatibility complex class I; MR, middle region; MVB, multivesicular body; NefE4A, Nef $EEEE_{65}$→$AAAA_{65}$; PACS, phosphofurin acidic cluster sorting protein; PBMCs, peripheral blood mononuclear cells; PBS, phosphate-buffered saline; PDB, Protein Data Bank; ROI, region of interest; siRNA, small interfering RNA; TFE, 2,2,2-trifluorethanol; TfR, transferrin receptor; TGN, *trans*-Golgi network; YFP, yellow fluorescent protein.

INTRODUCTION

After human immunodeficiency virus type 1 (HIV-1) transmission, the acute phase of infection is manifest by a massive burst in viremia and viral cytopathicity that triggers the antiviral response (McMichael *et al.*, 2010). Initially, the innate immune response is mobilized, which induces expression of restriction factors to impede the virus (Geijtenbeek and Gringhuis, 2009). The innate immune response also shapes the subsequent action of the adaptive immune response, which requires major histocompatibility complex class I (MHC-I) molecules to present viral antigens on the surface of infected cells, targeting them for destruction by cytotoxic T lymphocytes (CTLs; Lieberman, 2003).

HIV-1 uses several mechanisms to combat the antiviral response. The accessory proteins Vif and Vpu blunt the innate immune response by targeting destruction of APOBEC 3G and tetherin, respectively (Kirchhoff, 2010). HIV-1 uses two strategies to combat the adaptive immune response. One is the production of CTL escape mutants, which are generated by the low fidelity of HIV-1 replication (Sarmady *et al.*, 2011). This escape mechanism, however, is ultimately exhausted by the unsustainable cost to viral fitness (Friedrich *et al.*, 2004). The

accompanying strategy involves the down-regulation of cell-surface MHC-I. Indeed, the extent of MHC-I down-regulation in simian immunodeficiency virus-1–infected macaques correlates directly with the severity of disease progression, suggesting an important role for this immune-evasive mechanism in vivo (Friedrich *et al.*, 2010).

HIV-1 relies on the 27-kDa N-myristoylated accessory protein Nef to down-regulate MHC-I (Peterlin and Trono, 2003). Nef is required for the onset of acquired immune deficiency syndrome and can affect cells in many ways, including alteration of T cell activation and maturation, promotion of viral infectivity, subversion of the apoptotic machinery, and down-regulation of cell-surface molecules, including MHC-I (Fackler and Baur, 2002). Surprisingly, Nef controls these diverse processes using a limited number of sites that combine to bind >40 cellular proteins and multienzyme complexes, enabling the virus to subvert posttranscriptional programs as well as key steps in intracellular signaling and endocytic membrane traffic (Sarmady *et al.*, 2011). However, little is known about the biochemistry underlying most Nef–host protein interactions, precluding an understanding of how Nef drives HIV-1 disease.

To down-regulate MHC-I, Nef directs a temporally regulated program that uses at least four evolutionarily conserved sites—M_{20}, the $EEEE_{65}$ acidic cluster, and the $PXXP_{75}$ SH3-domain binding site, all of which are located in the N-terminal flexible region, and P_{78} (Lee *et al.*, 1996; Casartelli *et al.*, 2006; Dikeakos *et al.*, 2010). During the first 2 d after infection, Nef down-regulates MHC-I by an endocytic program called the signaling mode (Dikeakos *et al.*, 2010). This mode is initiated by the $EEEE_{65}$-dependent binding to the sorting protein PACS-2, which targets Nef to the paranuclear region, enabling $PXXP_{75}$ to direct assembly of an SFK/ZAP-70/PI3K complex that accelerates endocytosis of cell-surface MHC-I (Blagoveshchenskaya *et al.*, 2002; Hung *et al.*, 2007; Atkins *et al.*, 2008). Internalized MHC-I is then sequestered in paranuclear compartments by subversion of endocytic trafficking steps, which requires the $EEEE_{65}$-dependent binding to PACS-1 as well as Nef M_{20} and the heterotetrameric adaptor AP-1 (Blagoveshchenskaya *et al.*, 2002; Roeth *et al.*, 2004; Noviello *et al.*, 2008; Dikeakos *et al.*, 2010). By 3 d postinfection, Nef switches to the stoichiometric mode of down-regulation that prevents delivery of newly synthesized MHC-I molecules to the cell surface (Dikeakos *et al.*, 2010). Pharmacological inhibition of the signaling mode blocks onset of the stoichiometric mode, suggesting a key role for the PACS proteins in Nef-induced MHC-I down-regulation. This time course of the switch in Nef action suggests that HIV-1 may use the signaling and stoichiometric modes to down-regulate MHC-I in a reservoir-specific manner. For example, the ~1.5-d lifespan of an HIV-1–infected $CD4^+$ T cell suggests that Nef relies on the signaling mode to down-regulate MHC-I in this short-lived reservoir, whereas in longer-lived reservoirs, including cells of the monocytic lineage, Nef may sequentially employ the signaling mode, followed by the stoichiometric mode (Dikeakos *et al.*, 2010). The role of P_{78} has not been reported.

The PACS proteins are multifunctional homeostatic regulators expressed in metazoans that integrate secretory pathway traffic and interorganellar communication in healthy cells, with key steps in death ligand–induced apoptosis in diseased cells (Aslan *et al.*, 2009; Youker *et al.*, 2009). Lower metazoans express a single PACS gene, whereas higher metazoans express the PACS-1 and PACS-2 genes (Youker *et al.*, 2009). *Caenorhabditis elegans* PACS localizes to early endosomes and was identified in a genetic screen as a mediator of synaptic transmission (Sieburth *et al.*, 2005). In mammalian cells, PACS-1 mediates the *trans*-Golgi network (TGN) localization of furin and other cargo proteins that contain acidic cluster binding sites (Wan *et al.*, 1998; Crump *et al.*, 2001, 2003; Bouard *et al.*, 2007; Youker *et al.*, 2009). PACS-1 also mediates recycling of internalized cargo from early endosomes to the cell surface and trafficking to the primary cilium (Molloy *et al.*, 1998; Schermer *et al.*, 2005; Chen *et al.*, 2009; Jenkins *et al.*, 2009). PACS-2 mediates the localization of protein cargo to the endoplasmic reticulum and trafficking of endocytosed cargo from early endosomes to the TGN (Kottgen *et al.*, 2005; Atkins *et al.*, 2008; Myhill *et al.*, 2008).

The 150–amino acid PACS-1 and PACS-2 cargo (furin)-binding regions (FBRs) bind cargo proteins, sorting adaptors, and cellular kinases (Youker *et al.*, 2009). Whereas sites that bind sorting adaptors and kinases have been identified, the sites that bind cargo have not. Moreover, mutation of Nef $EEEE_{65}$ only reduces binding to PACS proteins, suggesting that their interaction is multivalent (Atkins *et al.*, 2008). Here we identify a conserved site in the PACS-1 and PACS-2 FBRs that interacts with a bipartite site on Nef formed by the $EEEE_{65}$ acidic cluster on the N-terminal domain and W_{113} in the Nef core domain. Mutation of this bipartite site disrupts the interaction with PACS proteins and correspondingly blocks Nef trafficking and MHC-I down-regulation. We also report the role of Nef P_{78} in binding PACS proteins and mediating Nef function. Our results provide new insight into the molecular basis of Nef action and suggest new strategies to combat HIV-1.

RESULTS

Identification of residues in the PACS-1 and PACS-2 FBRs required for binding Nef

Ab initio modeling predicts that the PACS-1 FBR (residues 117–266) is a loosely packed structure composed of long, flexible loops interspersed with several defined secondary structure elements (Youker *et al.*, 2009). The sites in PACS-1 important for binding the AP-1 heterotetramer ($ETELQLTF_{175}$), the monomeric adaptor GGA3 (KIY_{251}), or the protein kinase CK2 β-subunit ($RRKRY_{200}$) reside in ordered regions located on different surfaces of the predicted structure (Crump *et al.*, 2001; Scott *et al.*, 2006; Youker *et al.*, 2009; Figure 1A). The cargo-binding sites, however, have not been identified. The PACS-1 FBR binds the furin cytosolic domain at the CK2-phosphorylated acidic cluster $EECPpS_{773}DpS_{775}EEDE$ (Wan *et al.*, 1998). By contrast, the HIV-1 Nef acidic cluster $EEEE_{65}$, which is required for maximal binding of Nef to PACS-1 or PACS-2, lacks a CK2 site, suggesting that PACS proteins may bind Nef and furin differently. Consistent with this possibility, glutathione *S*-transferase (GST)–tagged PACS-$1_{117\text{-}266}$ bound hexahistidine (His_6)-tagged furin containing $S_{773}S_{775}$→DD phosphomimetic mutations (furin-DD) more robustly than His_6-Nef in vitro (Figure 1C). Correspondingly, a yeast two-hybrid analysis showed PACS-$1_{117\text{-}266}$ interacted with furin-DD but not Nef (Figure 1B).

The relatively weak binding between Nef and PACS-$1_{117\text{-}266}$ in vitro, together with the lack of a detectable interaction between these two molecules using the two-hybrid assay, raised the possibility that misfolded sequences within the PACS-1 FBR selectively interfered with the Nef-binding site. Consistent with this possibility, protein stability algorithms predicted the PACS-1 FBR is largely disordered but contains a stable region between residues 181 and 240 (Guruprasad *et al.*, 1990). To determine whether this stable region would be sufficient to interact with Nef, we tested the ability of PACS-1 FBR segments spanning residues 117–180, 181–240, and 241–266 to interact with Nef or furin-DD (Figure 1B). We found that Nef and furin-DD interacted robustly with PACS-$1_{181\text{-}240}$ but not with PACS-$1_{117\text{-}180}$ or PACS-$1_{241\text{-}266}$, suggesting that disordered regions flanking PACS-1 FBR residues 181–240 selectively interfered with binding to Nef. Further truncation analyses revealed that Nef interacted with PACS-$1_{181\text{-}195}$. Deletion of the C-terminal Q_{195}, however, blocked the interaction of PACS-$1_{181\text{-}194}$ with Nef.

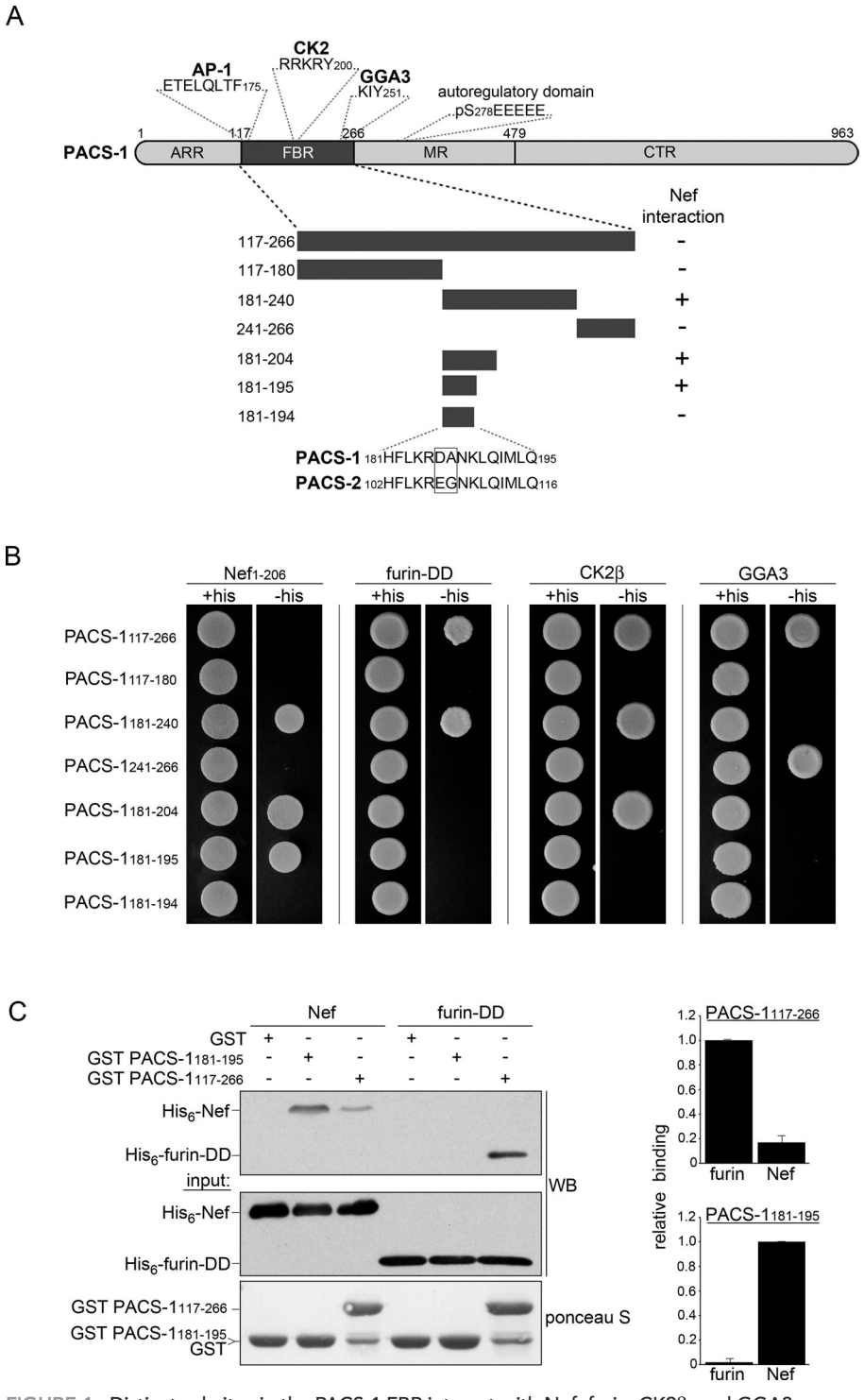

FIGURE 1: Distinct subsites in the PACS-1 FBR interact with Nef, furin, CK2β, and GGA3. (A) Top, schematic of PACS-1 depicting the atrophin-1–related region (ARR), FBR, middle region (MR) and C-terminal region (CTR), as well as the autoregulation site and sites required for binding AP-1, CK2, and GGA3. Middle, schematic of PACS-1 FBR deletion constructs tested in the two-hybrid screen. Left, amino acid residues; right, interaction of each construct with Nef (+, interaction; –, no interaction). Bottom, sequence alignment of PACS-$1_{181\text{-}195}$ with homologous PACS-$2_{102\text{-}116}$. Nonidentical residues are boxed. (B) Yeast cotransformed with bait plasmids expressing the indicated PACS-1 fragments and prey plasmids expressing Nef, the furin cytosolic domain containing $S_{773}S_{775}$→DD phosphomimetic mutations (furin-DD), CK2β, or GGA3 were screened for growth on His^+ or His^- media supplemented with 5 mM 3AT. (C) GST-PACS-$1_{181\text{-}195}$, GST-PACS-$1_{117\text{-}266}$, or GST alone was incubated with His_6-Nef or His_6-fur in-DD. GST proteins were captured, and bound His_6-Nef or His_6-furin-DD was detected by Western blot. Interactions were assayed in triplicate, and results are presented as the mean ± SD.

As controls, we analyzed the ability of the PACS-1 FBR segments to interact with CK2β or GGA3 (Figure 1B). In agreement with previous studies, CK2β interacted with PACS-$1_{181\text{-}204}$ but not PACS-$1_{181\text{-}195}$, consistent with the importance of the PACS-1 $RRKRY_{200}$ polybasic segment for the interaction of PACS-1 with CK2β (Scott *et al.*, 2006). In addition, GGA3 interacted only with PACS-$1_{241\text{-}266}$, which contains the KIY_{251} GGA3-binding site (Scott *et al.*, 2006).

To test whether PACS-$1_{181\text{-}195}$ could bind Nef, we conducted an in vitro protein capture assay (Figure 1C). His_6-tagged Nef or furin-DD was mixed with GST-tagged PACS-$1_{117\text{-}266}$ or PACS-$1_{181\text{-}195}$ or with GST alone. GST proteins were captured, and bound Nef or furin-DD was detected by Western blot. As expected, PACS-$1_{117\text{-}266}$ bound furin-DD approximately sevenfold greater than Nef. By contrast, PACS-$1_{181\text{-}195}$ bound Nef but not furin-DD. Together these experiments suggest that PACS-1 robustly binds furin and Nef and that disordered regions in the FBR selectively interfere with the Nef subsite.

Next we conducted an alanine scan to identify which residues in PACS-$1_{181\text{-}195}$ were required for interaction with full-length Nef ($Nef_{1\text{-}206}$; Figure 2A, top). Poly-alanine substitution of D_{186}-K_{189} but not H_{181}-R_{185} blocked the interaction between PACS-$1_{181\text{-}195}$ and Nef. Accordingly, a single alanine scan from PACS-1 D_{186} to Q_{195} showed that N_{188}, K_{189}, and Q_{195} were required for the interaction between PACS-$1_{181\text{-}195}$ and Nef. To determine whether mutational inactivation of the Nef:PACS-$1_{181\text{-}195}$ interaction in the two-hybrid assay reflected a direct block in protein–protein binding, we conducted in vitro protein capture assays. In agreement with the yeast two-hybrid analysis, His_6-Nef bound GST-tagged PACS-$1_{181\text{-}195}$ but not GST-tagged PACS-$1_{181\text{-}195}$ containing N_{188}→A or K_{189}→A substitutions (Figure 2B and Supplemental Figure S1). Because the PACS-1 N_{188}→A and K_{189}→A substitutions blocked Nef binding equally, subsequent analyses focused on the N_{188}→A mutation. To determine whether PACS-1 Asn_{188} was required for interaction between the corresponding full-length proteins in mammalian cells, we conducted coimmunoprecipitation analyses (Figure 2C). We coexpressed Nef-eYFP with hemagglutinin (HA)-tagged PACS-1 or PACS-1N_{188}A. PACS-1 proteins were immunoprecipitated, and coprecipitating Nef was detected by Western blot. In agreement with the yeast two-hybrid analyses, Nef interacted more efficiently with PACS-1 than

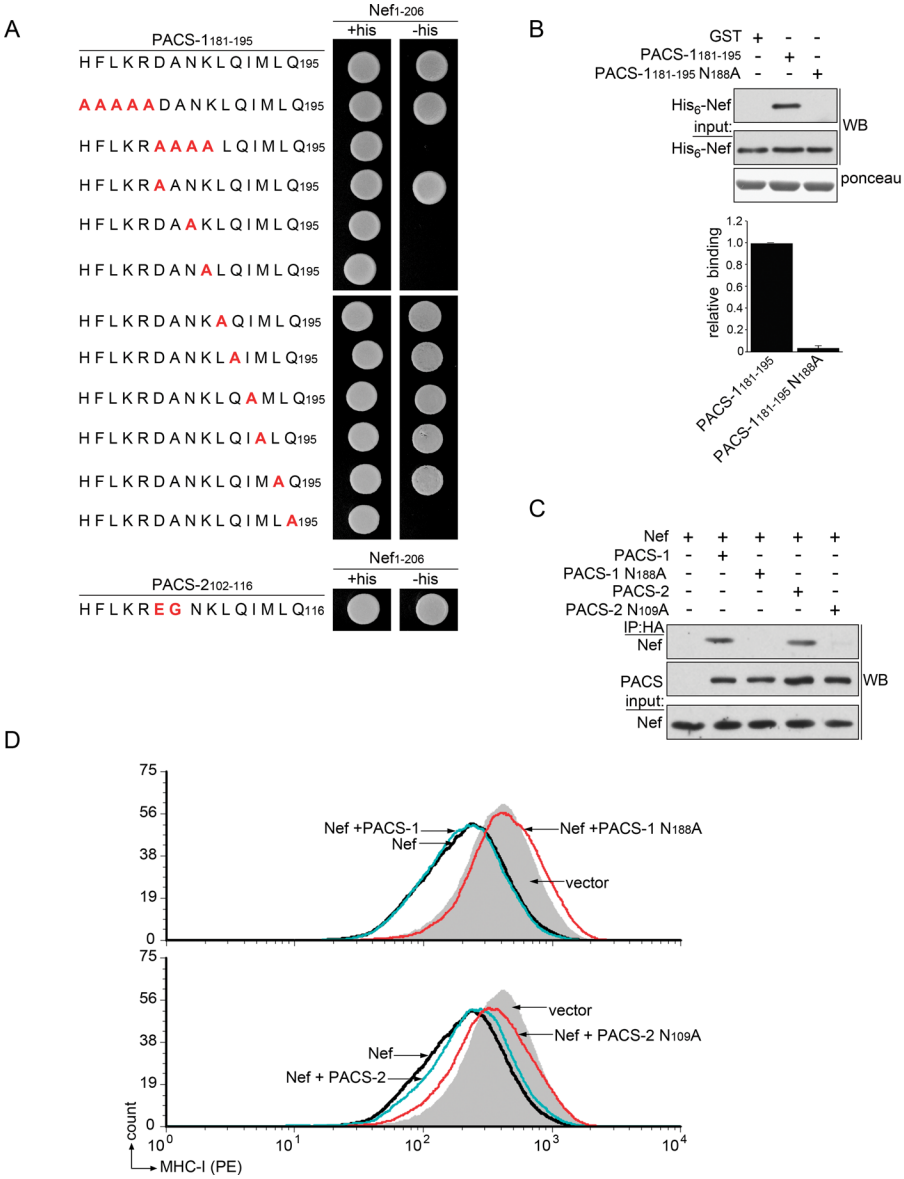

FIGURE 2: PACS-1 N_{188} and PACS-2 N_{109} are required for interacting with Nef and for Nef-induced MHC-I down-regulation. (A) Top, yeast cotransformed with bait plasmids expressing PACS-$1_{181-195}$ containing stepwise alanine mutations (mutated residues colored red) and a prey plasmid expressing full-length Nef (Nef$_{1-206}$) were screened for growth on His$^+$ or His$^-$ media supplemented with 5 mM 3AT. Bottom, yeast cotransformed with a bait plasmid expressing PACS-$2_{102-116}$ and a prey plasmid expressing full-length Nef were screened for growth on His$^+$ or His$^-$ media supplemented with 5 mM 3AT. (B) GST-PACS-$1_{181-195}$, GST-PACS-$1_{181-195}N_{188}$A, or GST alone was incubated with His_6-Nef. GST proteins were captured, and bound His_6-Nef was detected by Western blot. Protein capture was assayed in triplicate, and results are presented as the mean ± SD. (C) HeLa cells expressing Nef-eYFP alone or coexpressing Nef-eYFP and the indicated HA-tagged PACS proteins were lysed and HA-tagged proteins immunoprecipitated; coimmunoprecipitating Nef was detected by Western blot. (D) Top, H9 cells were nucleofected with plasmids expressing eYFP (vector, gray) or Nef-eYFP alone (Nef, black) or coexpressing Nef-eYFP and PACS-1 (blue) or PACS-1N_{188}A (red). At 40 h postnucleofection, cultures were fixed and eYFP$^+$ cells analyzed for cell-surface MHC-I (mAb W6/32) by flow cytometry. Bottom, H9 cells were nucleofected with plasmids expressing eYFP (vector, gray) or Nef-eYFP alone (Nef, black) or coexpressing Nef-eYFP and PACS-2 (cyan) or PACS-2N_{109}A (red). At 40 h postnucleofection, cultures were fixed and eYFP$^+$ cells analyzed for cell-surface MHC-I (mAb W6/32) by flow cytometry.

with PACS-1N_{188}A. Moreover, PACS-1 Asn_{188} appeared to be selectively required for the interaction of PACS-1 with Nef compared with other client proteins, since the N_{188}→A substitution blocked the interaction of PACS-$1_{181-240}$ with Nef but not with CK2β or furin-DD (Supplemental Figure S2 and Figure 1).

The PACS-$1_{181-195}$ sequence is nearly identical to the corresponding sequence located between residues 102 and 116 in the PACS-2 FBR, except that DA_{187} in PACS-1 is substituted by EG_{108} in PACS-2 (Figure 1A). To test whether Nef could interact with the PACS-2 FBR, we generated a PACS-$1_{181-195}$ construct containing the DA_{187}→EG substitution present in PACS-2. We found no difference in the interaction between Nef and PACS-$1_{181-195}$ or PACS-$2_{102-116}$, suggesting that Nef binds the same sites in the PACS-1 and PACS-2 FBRs (Figure 2A, bottom). Because PACS-1 N_{188} was required for the interaction of PACS-1 with Nef, we then asked whether PACS-2 N_{109}, which corresponds to PACS-1 N_{188}, was similarly required for the interaction with Nef in vivo. A coimmunoprecipitation analysis showed that Nef-eYFP interacted with HA-tagged PACS-2 but not with PACS-2N_{109}A (Figure 2C).

The repressed interaction between Nef and PACS-1N_{188}A or PACS-2N_{109}A raised the possibility that one or both of these mutant PACS proteins would interfere with Nef-induced down-regulation of MHC-I. To test this, we transfected H9 T cells with plasmids expressing eYFP (vector) or Nef-eYFP alone or cotransfected them with plasmids expressing Nef-eYFP and either PACS-1, PACS-1N_{188}A, PACS-2, or PACS-2N_{109}A (Figure 2D). We found that Nef-induced MHC-I down-regulation was markedly repressed by PACS-1N_{188}A, as well as by PACS-2N_{109}A, suggesting that these mutants disturbed Nef action by interfering with binding of Nef to endogenous PACS proteins.

Nef interacts with PACS-1 and PACS-2 on distinct endosomal populations

Identification of residues in the PACS-1 or PACS-2 FBRs required for the interaction with Nef provided an opportunity to visualize the subcellular location of the interaction between Nef and PACS-1 or PACS-2 using bimolecular fluorescence complementation (BiFC; Kerppola, 2008). Cells coexpressing BiFC reporter proteins composed of PACS-1 fused to the nonfluorescent yellow fluorescent protein (YFP) N-terminal fragment (PACS-1-Yn) or Nef fused to the nonfluorescent YFP carboxy-terminal fragment (Nef-Yc) displayed a dispersed cytoplasmic punctate staining pattern (Figure 3A). By contrast, coexpression of Nef-Yc with PACS-1N_{188}A-Yn generated a markedly reduced BiFC signal despite similar levels of expression, suggesting that the fluorescent signal generated by coexpression of Nef-Yc with PACS-1-Yn represented a bona fide

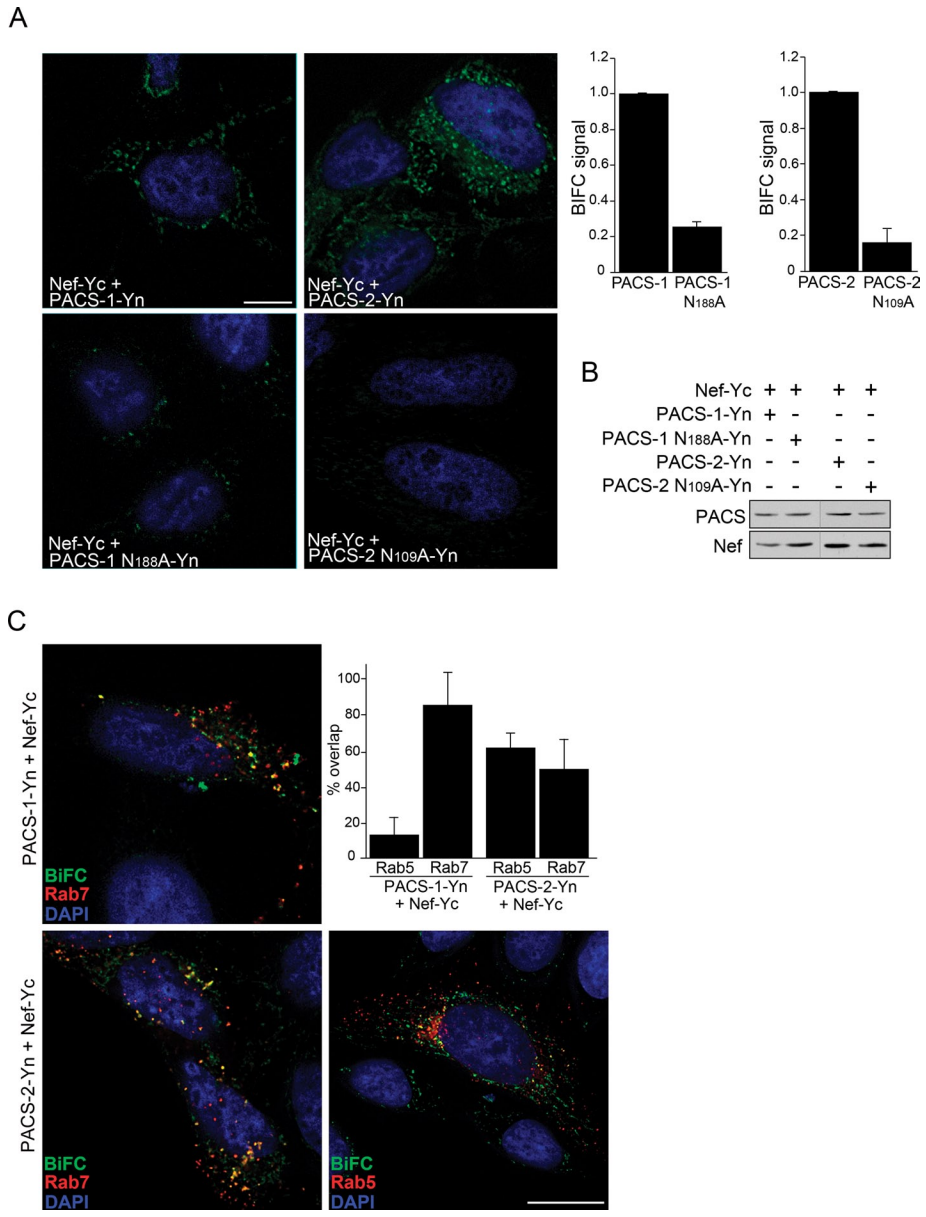

FIGURE 3: Nef interacts with PACS-1 and PACS-2 on distinct endosome populations. (A) Left, HeLa cells coexpressing Nef-Yc and PACS-1-Yn, PACS-2-Yn, PACS-1N_{188}A-Yn, or PACS-2N_{109}A-Yn for 24 h were fixed and counterstained with DAPI (blue), and the resulting BiFC signal (green) was captured on a high-resolution, wide-field Core DeltaVision system. Scale bar, 10 μm. Right, the BiFC signals generated by coexpression of Nef-Yc with PACS-1-Yn, PACS-2-Yn, PACS-1N_{188}A-Yn, or PACS-2N_{109}A-Yn from a minimum of 100 cells in three independent experiments were determined as described in *Materials and Methods* and quantified and presented as the mean ± SD. (B) HeLa cells coexpressing the indicated constructs were harvested, and the level of Nef-Yc and PACS-1-Yn, PACS-2-Yn, PACS-1N_{188}A-Yn, or PACS-2N_{109}A-Yn was measured by Western blot. (C) HeLa cells coexpressing Nef-Yc together with PACS-1-Yn and mcherry-Rab7 (upper left) or Nef-Yc together with PACS-2-Yn and either mcherry-Rab7 (lower left) or mcherry-Rab5 (lower right) for 24 h were fixed, counterstained with DAPI (blue), and analyzed for BiFC (green) or Rab proteins (red) using a high-resolution, wide-field Core DeltaVision system. Scale bar, 10 μm. Upper right, quantitation. The colocalization of the BiFC signal generated by coexpression of Nef-Yc with PACS-1-Yn or PACS-2-Yn with mcherry-tagged Rab5 or Rab7 proteins from a minimum of 35 cells in four independent experiments was quantified as described in *Materials and Methods* and is presented as the mean ± SD.

protein–protein interaction (Figure 3, A and B). Next we tested whether the interaction between Nef and PACS-2 could by visualized by BiFC. We detected a punctate BiFC signal in the cytoplasm of cells that coexpressed Nef-Yc with PACS-2 fused to the nonfluorescent YFP N-terminal fragment (PACS-2-Yn) but not with PACS-2N_{109}A-Yn (Figure 3, A and B). Singular expression of Nef-Yc, PACS-1Yn, or PACS-2Yn alone generated background BiFC signals similar to that obtained by coexpression of Nef-Yc with PACS-1N_{188}A-Yn or with PACS-2N_{109}A-Yn, consistent with the determination that the mutant PACS proteins generate only background interaction with Nef (unpublished data).

To test whether the punctate BiFC staining pattern represented the interaction of Nef and PACS proteins on endosomes, we coexpressed the BiFC reporter proteins with mcherry-Rab5, which decorates early endosomes, or mcherry-Rab7, which decorates multivesicular bodies (MVBs)/late endosomes (Figure 3C). We found that the BiFC signal generated by the interaction of Nef-Yc with PACS-1-Yn overlapped predominantly with mcherry-tagged Rab7 but not Rab5. By contrast, the BiFC signal generated by the interaction of Nef-Yc with PACS-2Yn overlapped with both mcherry-tagged Rab5 and Rab7. These findings suggest that Nef interacts with PACS-1 on MVB/late endosomes and with PACS-1 or PACS-2 on early endosomes.

Nef $EEEE_{65}$, P_{78}, and Y_{120} are involved in interacting with the PACS-1 FBR

The Nef acidic cluster $EEEE_{65}$ is required for MHC-I down-regulation and for maximal binding to PACS-1 or PACS-2 (Greenberg *et al.*, 1998; Piguet *et al.*, 2000; Atkins *et al.*, 2008). However, the $EEEE_{65}$→$AAAA_{65}$ (NefE4A) mutation only partially reduces binding to PACS proteins, suggesting that additional sites in Nef are required for maximal binding (Atkins *et al.*, 2008). To systematically identify Nef residues required for binding PACS proteins, we conducted a yeast two-hybrid screen to analyze the interaction between PACS-$1_{181-195}$ and a series of Nef truncation mutants (Figure 4A). As expected, PACS-$1_{181-195}$ interacted with Nef_{1-65} but not with Nef_{1-61} or Nef_{1-65}E4A (Figure 4B). Surprisingly, however, PACS-$1_{181-195}$ also interacted with Nef_{71-206}, suggesting that PACS-1 binds a second site in the Nef core domain (Figure 4C). An N-terminal truncation analysis showed that PACS-$1_{181-195}$ interacted with Nef_{77-206} but not Nef_{80-206}, suggesting that PACS-$1_{181-195}$ binding to Nef requires a site in the polyproline region C-terminal to the $PXXP_{75}$ site. Stepwise alanine substitution of Nef residues 77-79 revealed that only P_{78} was required for interaction of the Nef C-terminal region with PACS-$1_{181-195}$.

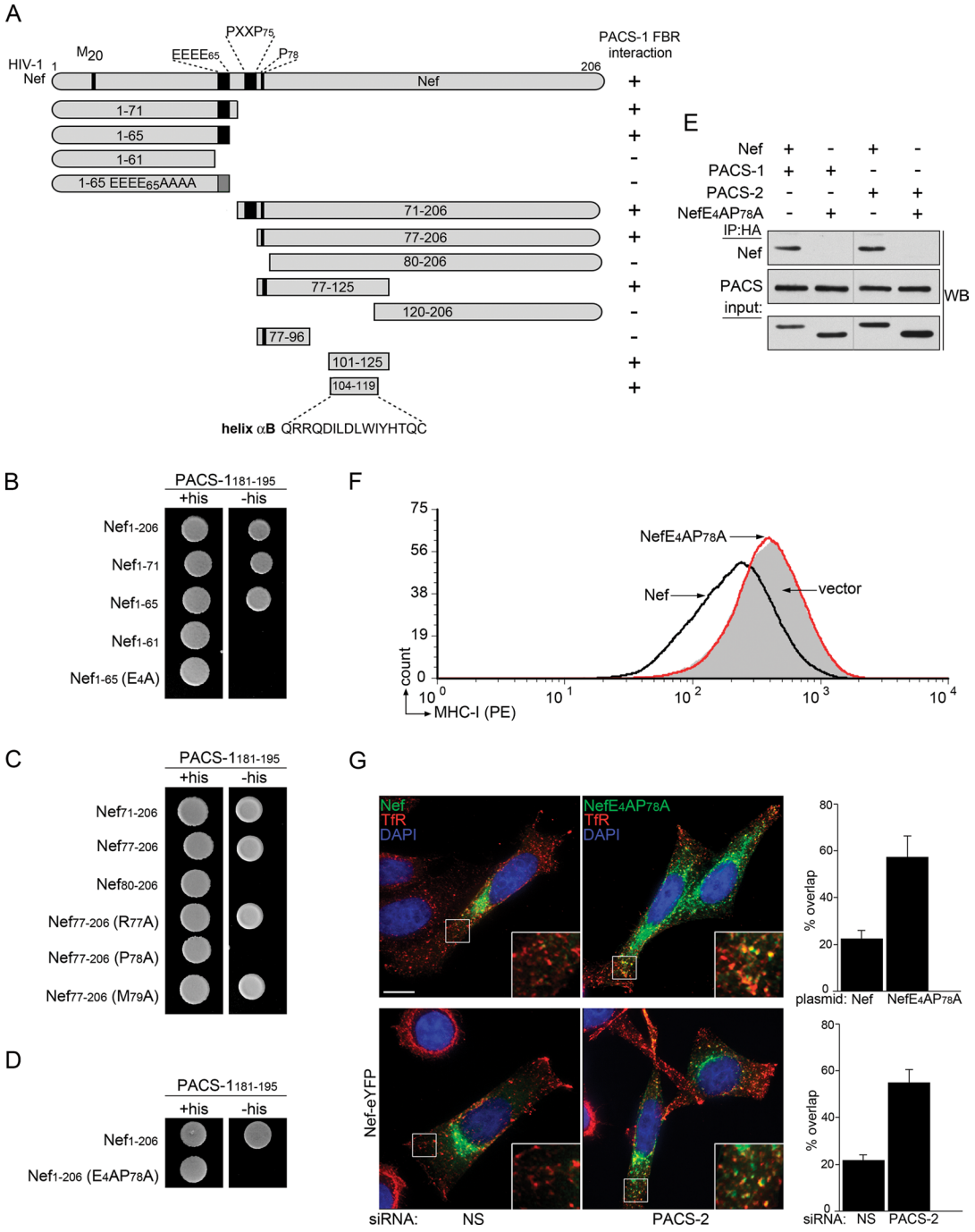

FIGURE 4: Nef EEEE$_{65}$ and Pro$_{78}$ are required for the interaction with PACS-1 and PACS-2. (A) Top, schematic of Nef depicting the M$_{20}$, EEEE$_{65}$, PXXP$_{75}$, and P$_{78}$ sites required for MHC-I down-regulation. Bottom, schematic of the Nef deletion constructs tested in the two-hybrid screen. Amino acid residues are presented in the stick diagrams, and interaction of each construct with PACS-1$_{181-195}$ is presented on the right (+, interaction; –, no interaction). (B–D) Yeast cotransformed with the bait plasmid expressing PACS-1$_{181-195}$ and prey plasmids expressing full-length Nef or the indicated Nef mutants were screened for growth on His$^+$ or His$^-$ media supplemented with 5 mM 3AT. (E) HeLa cells coexpressing eYFP-tagged Nef or NefE4AP$_{78}$A with either HA-tagged PACS-1 or PACS-2 as indicated were lysed, HA-tagged proteins immunoprecipitated, and coimmunoprecipitating Nef or NefE4AP$_{78}$A was detected by western blot. (F) H9 cells were nucleofected with plasmids expressing eYFP (vector, gray), Nef-eYFP (Nef, black), or NefE4AP$_{78}$A-eYFP (NefE4AP$_{78}$A, red). At 40 h postnucleofection, cultures were fixed and eYFP$^+$ cells analyzed for cell-surface MHC-I (mAb W6/32) by flow cytometry. (G) Top, HeLa cells expressing Nef-eYFP or NefE4AP$_{78}$A-eYFP for 40 h were fixed, incubated with anti-TfR (red), and counterstained with DAPI (blue). At 40 h postnucleofection, cells were fixed and stained for TfR (red), and images were captured using a high-resolution, wide-field Core DeltaVision system. Scale bar, 10 μm. Bottom, HeLa cells were transfected with a nonspecific siRNA (NS) or siRNA directed against PACS-2 for 24 h and then nucleofected with a plasmid expressing Nef-eYFP. At 40 h postnucleofection, cells were analyzed as described. Insets, magnification of boxed areas. Right, colocalization of TfR with Nef-eYFP or NefE4AP$_{78}$A-eYFP was quantified as described in *Materials and Methods*. Error bars represent the mean ± SD from 30 cells in three independent experiments.

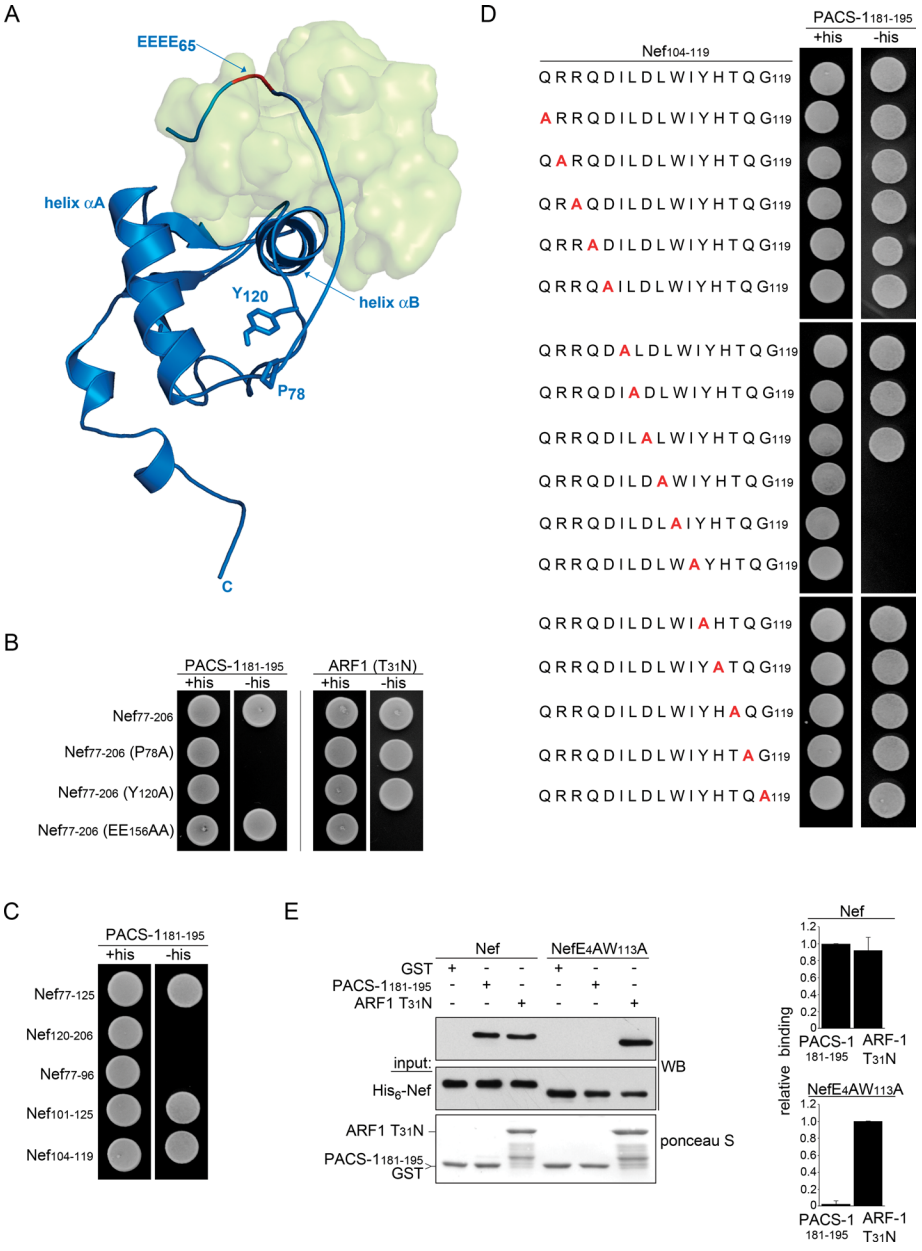

FIGURE 5: Interaction of the PACS-1 FBR with Nef helix αB. (A) Molecular docking of PACS-$1_{181-195}$ with Nef (PDB ID: 2Nef, blue). Light green surface images represent an ensemble of the cluster with the highest number of poses for the docking of PACS-$1_{181-195}$ to Nef. Nef $EEEE_{65}$ (red) and P_{78} and Y_{120} (sticks) are highlighted. (B) Yeast cotransformed with bait plasmids expressing PACS-$1_{181-195}$ (left) or ARF1T_{31}N (right) and prey plasmids expressing the indicated Nef constructs were screened for growth on His^+ or His^- media supplemented with 50 mM 3AT. (C) Yeast cotransformed with the bait plasmid expressing PACS-$1_{181-195}$ and prey plasmids expressing the indicated Nef constructs were screened for growth on His^+ or His^- media supplemented with 50 mM 3AT. (D) Yeast cotransformed with a bait plasmid expressing PACS-$1_{181-195}$ and prey plasmids expressing Nef residues 104–119 containing stepwise alanine mutations (mutated residues colored red) were screened for growth on His^+ or His^- media supplemented with 50 mM 3AT. (E) GST-PACS-$1_{181-195}$, GST-ARF1 T_{31}N, or GST alone was incubated with His_6-Nef or His_6-NefE4AW_{113}A. GST proteins were captured, and bound His_6-Nef or His_6-NefE4AW_{113}A was detected by Western blot. Interactions were assayed in triplicate, and results are presented as the mean ± SD.

We conducted several experiments to test the extent to which Nef $EEEE_{65}$ and P_{78} are required for interacting with PACS-1 or PACS-2 and for mediating PACS-dependent Nef action. We found in the yeast two-hybrid assay that PACS-$1_{181-195}$ interacted with full-length Nef (Nef_{1-206}) but not Nef-E4AP_{78}A, which contains the $EEEE_{65}$→AAAA and P_{78}→A double mutation (Figure 4D). Correspondingly, coimmunoprecipitation experiments in mammalian cells showed that PACS-1 and PACS-2 interacted with Nef but not Nef-E4AP_{78}A (Figure 4E). To test the effect of the E4AP_{78}A mutation on Nef-induced MHC-I down-regulation, we incubated H9 T-cells expressing eYFP-tagged Nef or Nef-E4AP_{78}A or eYFP alone with an anti-MHC-I antibody and analyzed them by flow cytometry. In agreement with the coimmunoprecipitation analysis, we found that cell-surface MHC-I was efficiently down-regulated by Nef but not by Nef-E4AP_{78}A (Figure 4F).

The failure of Nef-E4AP_{78}A to interact with PACS-1 and PACS-2 suggested that, in addition to an inability to down-regulate MHC-I, this Nef mutant would be blocked in PACS-dependent trafficking. In agreement with previous studies (Atkins *et al.*, 2008; Dikeakos *et al.*, 2010), Nef-eYFP expressed in HeLa cells accumulated in the Golgi region (Figure 4G). By contrast, Nef-E4AP_{78}A-eYFP accumulated largely in a dispersed population of transferrin receptor (TfR)–positive early endosomes. The subcellular distribution of Nef-E4AP_{78}A-eYFP was similar to the mislocalization of Nef-eYFP caused by PACS-2 small interfering RNA (siRNA) knockdown, which also caused Nef-eYFP to redistribute to a population of dispersed, TfR-positive early endosomes (Figure 4G and Supplemental Figure S3; Atkins *et al.*, 2008; Dikeakos *et al.*, 2010).

The PACS-1 FBR interacts with W_{113} in Nef helix αB

To gain insight into how Nef may bind PACS-1 and PACS-2, we used the ClusPro 2.0 server with unconstrained binding parameters to dock PACS-$1_{181-195}$ onto Nef (Protein Data Bank [PDB] ID: 2Nef; Grzesiek *et al.*, 1997; Kozakov *et al.*, 2010). The docked cluster with the most populated poses is shown in Figure 5A. The α-helical structure of PACS-$1_{181-195}$ portrayed in this analysis was consistent with ab initio modeling of the PACS-1 FBR and was supported empirically by circular dichroism (CD) spectroscopy of a synthetic peptide containing the PACS-1 residues N_{188}, K_{189}, and Q_{195} required for interaction with Nef (Youker *et al.*, 2009; Supplemental Figure S4). Because a peptide corresponding to PACS-1 181–195 was insoluble at neutral pH, we determined the secondary structure of the slightly offset 17-mer peptide corresponding to PACS-1 184–200. CD analysis showed that PACS-$1_{184-200}$ contained a small amount of helical structure that was abolished by the

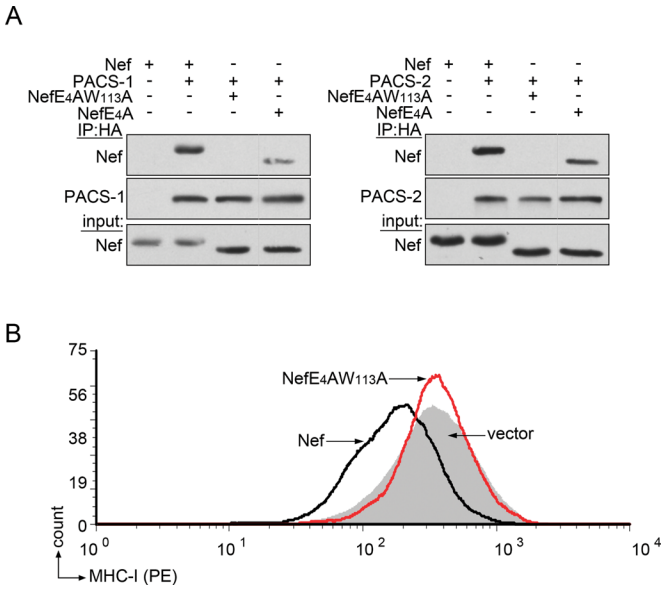

FIGURE 6: PACS-1 interacts with Nef $EEEE_{65}$ and W_{113}. (A) HeLa cells were nucleofected with plasmids coexpressing HA-tagged PACS-1 or PACS-2 with eYFP-tagged Nef, NefE4A, or NefE4AW_{113}A. After 24 h, cells were lysed and HA-tagged proteins immunoprecipitated; coimmunoprecipitating Nef proteins were detected by Western blot. (B) H9 cells were nucleofected with plasmids expressing eYFP (vector, gray), Nef-eYFP (Nef, black), or NefE4AW_{113}A-eYFP (NefE4AP_{78}A, red). At 40 h postnucleofection, cultures were fixed and $eYFP^+$ cells analyzed for cell-surface MHC-I (mAb W6/32) by flow cytometry.

denaturant urea and increased by the α-helix stabilizer 2,2,2-trifluorethanol (TFE; Luo and Baldwin, 1997).

The docked poses generated by the ClusPro 2.0 server suggested that PACS-$1_{181\text{-}195}$ could interact with a bipartite site in Nef composed of $EEEE_{65}$ and helix αB in the core domain but not with P_{78} (Figure 5A). Of interest, the HIV-1 Nef structure reveals that P_{78} packs against Y_{120}, which stabilizes the Nef core region by capping helix αB (Lee *et al.*, 1996). Consistent with the structural data, a yeast two-hybrid analysis showed that P_{78}→A or Y_{120}→A substitutions each blocked the interaction of $Nef_{77\text{-}206}$ with PACS-$1_{181\text{-}195}$ (Figure 5B, left). By contrast, neither the P_{78}→A nor the Y_{120}→A substitution interfered with the interaction of $Nef_{77\text{-}206}$ with Arf1T_{31}N, which interacts with Nef EE_{156} (Figure 5B, right; Faure *et al.*, 2004). Conversely, a Nef EE_{156}→AA substitution blocked interaction of Nef with Arf1T_{31}N but not PACS-$1_{181\text{-}195}$. Together these findings suggest that P_{78} promotes interaction of Nef with PACS proteins not by binding PACS-1 but by interacting with Y_{120}, which stabilizes the structural integrity of the Nef core domain required for binding PACS-1.

In support of the possibility that PACS-1 interacts with Nef helix αB, we found that PACS-$1_{181\text{-}195}$ interacted with $Nef_{77\text{-}125}$ but not $Nef_{120\text{-}206}$ (Figure 5C). Further analyses showed that PACS-$1_{181\text{-}195}$ interacted robustly with $Nef_{104\text{-}119}$, which corresponds to helix αB, but not with $Nef_{77\text{-}96}$, which corresponds to helix αA. To identify specific residues in Nef helix αB required for interaction with PACS-$1_{181\text{-}195}$, we conducted a single-alanine scan of Nef residues 104–119 and found that mutation of L_{112}, W_{113}, or I_{114} blocked interaction with PACS-$1_{181\text{-}195}$ (Figure 5D). To test whether this hydrophobic cluster was required for binding Nef to PACS-1 in vitro, we incubated GST-tagged PACS-$1_{181\text{-}195}$ with His_6-tagged Nef or Nef-E4AW_{113}A. As a control, we tested the binding of GST-tagged Arf1T_{31}N to His_6-tagged Nef or Nef-E4AW_{113}A. In agreement with the yeast two-hybrid analysis, we found that Nef bound Arf1T_{31}N and PACS-$1_{181\text{-}195}$, whereas Nef-E4AW_{113}A bound Arf1T_{31}N but not PACS-$1_{181\text{-}195}$ (Figure 5E).

To test whether the hydrophobic cluster in Nef helix αB was required for interacting with full-length PACS proteins, we coexpressed HA-tagged PACS-1 or PACS-2 with Nef, NefE4A, or Nef-E4AW_{113}A. The PACS proteins were immunoprecipitated, and coprecipitating Nef proteins were detected by Western blot. In agreement with previous studies, the PACS proteins interacted with Nef and to a lesser extent with NefE4A (Figure 6A; Atkins *et al.*, 2008). However, similar to our results for Nef-E4AP_{78}A (Figure 4), the PACS proteins failed to coimmunoprecipitate Nef-E4AW_{113}A. Because PACS-2-mediated trafficking of Nef to the Golgi region is required for the $PXXP_{75}$-dependent interaction of Nef with SFKs (Atkins *et al.*, 2008), we asked whether the E4AW_{113}A mutation would affect the interaction with Hck. We found that Hck was readily coimmunoprecipitated with Nef but not Nef-E4AW_{113}A (Supplemental Figure S5). To test the effect of the E4AW_{113}A mutation on MHC-I down-regulation, we conducted two experiments. First, H9 T cells expressing eYFP-tagged Nef or Nef-E4A W_{113}A or eYFP alone (vector) were incubated with an anti-MHC-I antibody and analyzed by flow cytometry. In agreement with the coimmunoprecipitation analysis, we found that cell-surface MHC-I was efficiently down-regulated by Nef but not by Nef-E4AW_{113}A (Figure 6B). To determine whether the $EEEE_{65}$ and W_{113} sites were required for Nef-induced MHC-I down-regulation in primary target cells, PBMCs were nucleofected with plasmids expressing eYFP-tagged Nef or Nef-E4AW_{113}A or eYFP alone (vector), and the extent of HLA-A2.1 down-regulation was monitored by flow cytometry (Supplemental Figure S6). In agreement with the studies in H9 T cells, the E4AW_{113}A mutation markedly repressed Nef-induced down-regulation of HLA-A2.1.

Mutation of the PACS-binding site disrupts Nef trafficking

We asked to what extent the failure of Nef-E4AW_{113}A to interact with PACS proteins would affect its trafficking and found that this Nef mutant failed to localize to the Golgi region (Figure 7, A and B). Whereas Nef-E4AW_{113}A-eYFP and Nef-E4AP_{78}A-eYFP were both redistributed to cortical TfR- and mcherry-Rab5–positive early endosomes, Nef-E4AW_{113}A-eYFP expression induced accumulation of tubular- and donut-shaped endosomal structures (compare Figures 4G and 7A). We found that Nef-E4AW_{113}A-eYFP colocalized predominantly with mcherry-Rab7 in donut-shaped compartments, suggesting that they were a population of MVB/late endosomes (Figure 7, A and C). By contrast, Nef-E4AW_{113}A-eYFP was predominantly found in Rab5-positive tubular structures, possibly reflecting a population of tubulated early endosomes. Structured illumination microscopy was used to more precisely resolve the subcellular localization of Nef-E4AW_{113}A-eYFP (Figure 7D, left). We found that tubule-localized Nef-E4AW_{113}A-YFP was frequently concentrated in varicosities that extended linearly from mcherry-Rab5–containing endosomes. By contrast, donut-localized Nef-E4AW_{113}A-YFP was frequently found apposed to or surrounding endosomal mcherry-Rab7 (Figure 7D, right). Together these findings suggest that $EEEE_{65}$ and W_{113} combine to mediate the interaction of Nef with PACS-1 or PACS-2, which is crucial for directing the TGN/endosomal trafficking of Nef and for the ability of Nef to down-regulate MHC-I.

Bipartite binding sites direct the interaction of Nef with PACS proteins

The identification of specific sites on the PACS proteins and HIV-1 Nef necessary and sufficient for their interaction and for Nef-induced MHC-I down-regulation prompted us to ask to what extent the molecular docking analysis was consistent with the empirical data. Of

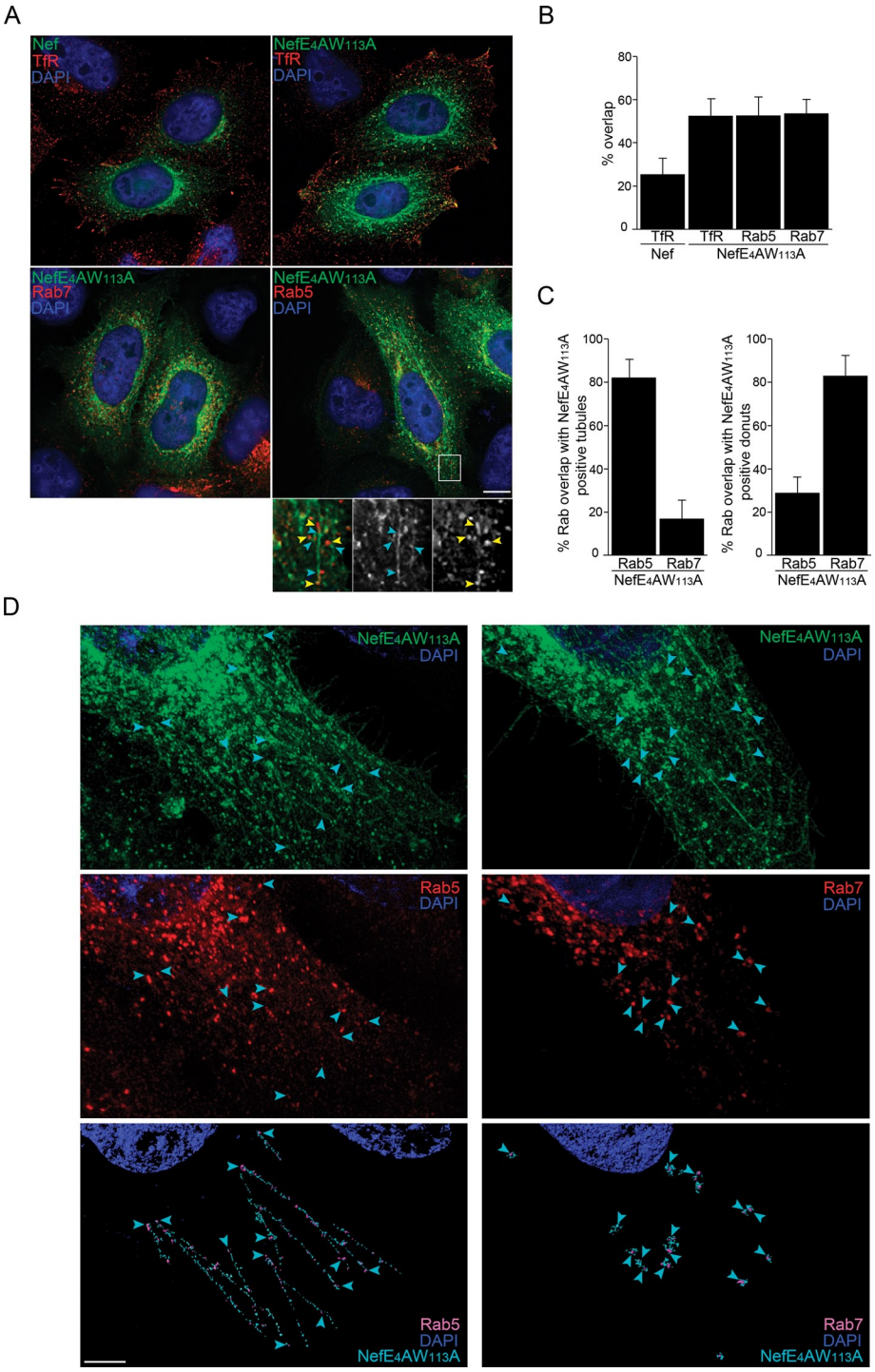

FIGURE 7: Mutation of the PACS-binding site disrupts Nef trafficking. (A) Top, HeLa cells expressing Nef-eYFP or NefE4AW$_{113}$A-eYFP for 40 h were fixed, incubated with anti-TfR (red), and counterstained with DAPI (blue), and images were captured using a high-resolution, wide-field Core DeltaVision system. Middle, HeLa cells were nucleofected with plasmids expressing Nef-eYFP or NefE4AW$_{113}$A-eYFP alone or coexpressing the eYFP-tagged Nef constructs with either mcherry-Rab5 or mcherry-Rab7 as indicated. At 40 h postnucleofection, cells were fixed, incubated with anti-TfR (red) or not as indicated, and counterstained with DAPI (blue), and images were captured as described. Scale bar, 10 μm. Bottom, magnification of the boxed region from the panel above (right), together with the black and white images of the NefE4AW$_{113}$A-eYFP signal (middle) and the mcherry-Rab5 signal (right). Blue arrowheads, NefE4AW$_{113}$A-eYFP. Yellow arrowheads, mcherry-Rab5. (B) Colocalization of Nef-eYFP or NefE4AW$_{113}$A-eYFP with each endocytic marker was determined as described in *Materials and Methods*. Error bars represent the mean ± SD from at least 50 cells from three (mcherry-tagged Rab 5 or Rab7) or four (TfR) independent experiments. (C) Colocalization of mcherry-tagged Rab5 or Rab7 with NefE4AW$_{113}$A-eYFP–positive tubules (left graph) or donut-shaped structures (right graph) was quantified as described in *Materials and Methods*. Error bars represent the mean ± SD of at least 300 tubule or donut structures from three independent experiments. (D) HeLa cells from experiments described in A coexpressing NefE4AW$_{113}$A-eYFP (top) and mcherry-Rab5 (middle) or mcherry-Rab7 (middle) for 24 h were fixed and counterstained with DAPI (blue). Images were captured using structured illumination microscopy, and 3D surface representations were generated using Imaris (bottom). Representative Nef-E4AW$_{113}$A-eYFP–containing tubular (top left) or donut-shaped (top right) structures are highlighted with arrowheads. The arrowheads were then copied on to the middle images showing the mcherry-tagged Rab5 (left) or Rab7 (right) channels to maintain selection of the same structures. Highlighted compartments are pseudocolored for NefE4AW$_{113}$A-eYFP (cyan) or mcherry-Rab proteins (magenta). Scale bar, 5 μm. The discrete compartments depicted in the model of tubular Nef-E4AW$_{113}$A-eYFP likely reflect varicosities along the tubule enriched in Nef-E4AW$_{113}$A-eYFP, since the tubules are frequently continuous in the raw image. The apparent breaks in the tubules reflect the signal detection limits used for the 3D image processing.

interest, one Nef:PACS-1$_{181\text{-}195}$ pose suggested that PACS-1 NK$_{189}$ (corresponding to PACS-2 NK$_{110}$) was included in an α-helical segment with aliphatic chains abutted against W$_{113}$ in HIV-1 Nef (Figures 8A and Supplemental Figure S4). Moreover, the docking model was also consistent with the ability of PACS-1$_{181\text{-}195}$ containing a conservative N$_{188}$→Q substitution to interact with Nef$_{104\text{-}119}$ containing a conservative W$_{113}$→F substitution (Figure 8, B–D). These findings suggest that the failure of the PACS-1 N$_{188}$→A and Nef W$_{113}$→A substitutions to support protein–protein binding likely resulted from the small Ala side-chain substitution rather than from a global disruption of protein structure (Figures 2 and 5).

The docking model further predicted that PACS-1 KR$_{185}$ (KR$_{106}$ in PACS-2) could interact with HIV-1 Nef EEEE$_{65}$. Because our initial analysis of the sites in PACS-1$_{181\text{-}195}$ required for interaction with Nef were conducted using full-length Nef (Nef$_{1\text{-}206}$), it raised the possibility that the interaction between Nef W$_{113}$ and PACS-1 NK$_{189}$ may have masked a weaker interaction between Nef EEEE$_{65}$ and PACS-1 KR$_{185}$. To test this, we systematically analyzed the interaction of a series of PACS-1$_{181\text{-}195}$ constructs

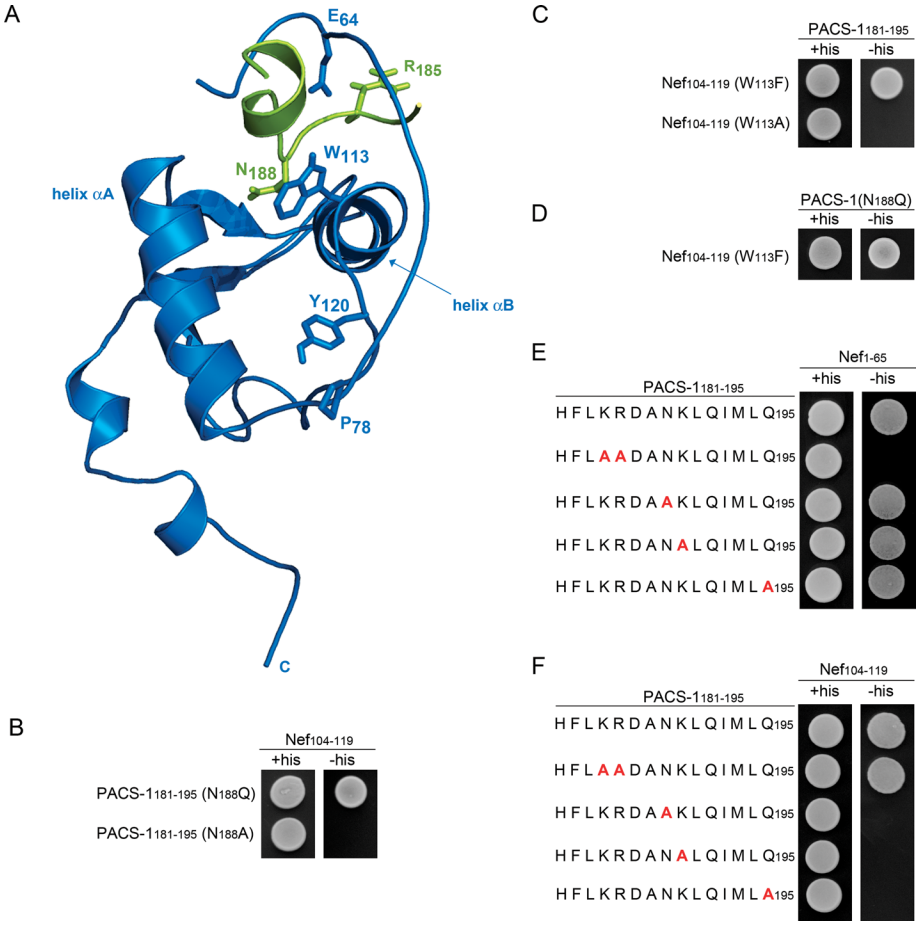

FIGURE 8. Identification of bipartite binding sites in PACS-1 and Nef that mediate protein–protein interaction. (A) Molecular docking of PACS-$1_{181-195}$ (green) with Nef (PDB ID: 2Nef, blue). PACS-1 amino acids R_{185} and N_{188} and Nef residues E_{64}, P_{78}, W_{113}, and Y_{120} (sticks) are highlighted. (B–D) Yeast cotransformed with plasmids expressing $Nef_{104-119}$ and PACS-$1_{181-195}N_{188}$A or PACS-$1_{181-195}N_{188}$Q (panel B), PACS-$1_{181-195}$, and $Nef_{104-119}W_{113}$F or $Nef_{104-119}W_{113}$A (C) or PACS-$1_{181-195}N_{188}$Q and $Nef_{104-119}W_{113}$F (D) were screened for growth on His^+ or His^- media supplemented with 50 mM 3AT. (E, F) Yeast cotransformed with the prey plasmids expressing Nef_{1-65} (E) or $Nef_{104-119}$ (F) and bait plasmids expressing the indicated PACS-1 alanine mutants (red) were screened for growth on His^+ or His^- media supplemented with 5 mM 3AT.

containing Ala substitutions at each residue with either Nef_{1-65}, which contains only the $EEEE_{65}$ site, or $Nef_{104-119}$, which contains only the W_{113} hydrophobic site. Mutation of PACS-1 N_{188}, K_{189}, or Q_{195} blocked the interaction with $Nef_{104-119}$ but not Nef_{1-65} (Figure 8E and Supplemental Figure S7). By contrast, mutation of PACS-1 KR_{185} blocked interaction of PACS-$1_{181-195}$ with Nef_{1-65} but not $Nef_{104-119}$ (Figure 8F and Supplemental Figure S7). Together these findings suggest that PACS proteins mediate Nef action by interaction between bipartite binding sites—one formed by KR_{185} and NK_{189} (PACS-1 numbering) located within a small, 15–amino acid helical segment in the PACS-1 and PACS-2 FBRs and the other formed by $EEEE_{65}$ in the Nef N-terminal flexible domain and W_{113} in helix αB in the Nef core.

DISCUSSION

The 150–amino acid PACS-1 and PACS-2 FBRs contain sites required for binding secretory pathway trafficking regulators, including AP-1, COPI, CK2, and GGA3, as well as a large number of cargo proteins that contain acidic cluster sorting motifs (Youker *et al.*, 2009). Despite the markedly different acidic cluster motifs on furin and Nef, these two cargo proteins interact with overlapping subsites in the PACS-1 and PACS-2 FBRs distinct from sites that interact with adaptors or CK2 (Figure 1). Here we identified a 15–amino acid segment of PACS-1 (residues 181–195) or PACS-2 (residues 102–116) sufficient to interact robustly with Nef; this interaction required residues N_{188} (N_{109} in PACS-2), K_{189}, and Q_{195}. Mutation of the essential asparagine residue in the Nef-binding site on PACS-1 or PACS-2 (PACS-$1N_{188}$A or PACS-$2N_{109}$A) blocked the interaction of PACS proteins with Nef on endosomal compartments and repressed Nef-induced MHC-I down-regulation (Figures 2 and 3). Correspondingly, the $NefE4AP_{78}$A and $NefE4AW_{113}$A mutants unable to bind PACS-1 or PACS-2 were blocked in PACS-dependent trafficking of Nef to the paranuclear region and in MHC-I down-regulation (Figures 4–7). Protein interaction assays showed that PACS-1 KR_{185} was required for interaction with Nef $EEEE_{65}$, whereas N_{188}, K_{189}, and Q_{195} were required for interaction with a hydrophobic site in the Nef core that included L_{112}, W_{113}, and I_{114} in helix αB (Figure 8). The conservation of the $EEEE_{65}$ and W_{113} sites from multiple HIV clades suggests a broad and essential role for the Nef–PACS interaction in driving Nef function (Lee *et al.*, 1996; Kirchhoff *et al.*, 1999; Ali *et al.*, 2010).

The PACS family of sorting proteins arose late in evolution and is expressed only in metazoans (Youker *et al.*, 2009). Of interest, *C. elegans* PACS localizes to early endosomal compartments, where it mediates trafficking steps controlling cell–cell communication (Sieburth *et al.*, 2005). Thus the interaction of HIV-1 Nef with PACS proteins on endosomal compartments as determined using BiFC suggests an evolutionarily conserved role for PACS-1 and PACS-2 in endosomal traffic (Figure 3). The colocalization of Nef with PACS-1 on a subpopulation of Rab7-positive endosomes is consistent with the role of PACS-1 in sequestering MHC-I molecules after their Nef-induced endocytosis and the determination that down-regulated MHC-I accumulates in Rab7-positive compartments (Schaefer *et al.*, 2008; Dikeakos *et al.*, 2010). By contrast, Nef interacted with PACS-2 on Rab5-positive early endosomes (Figure 3), which is consistent with the role of PACS-2 in trafficking Nef from peripheral early endosomes to the Golgi region, where it can assemble the multikinase complex that triggers MHC-I down-regulation (Atkins *et al.*, 2008).

The Nef proline-rich region mediates multiple steps in Nef-induced MHC-I down-regulation. P_{72} and P_{75} form a type II polyproline helix that binds the SH3 domains of SFKs (Lee *et al.*, 1996; Grzesiek *et al.*, 1997). This binding directly activates a subset of SFKs—Hck, Lyn, and Src—each of which can be assembled by Nef into the SFK/ZAP-70/PI3K multikinase complex that triggers MHC-I down-regulation (Dikeakos *et al.*, 2010). By contrast, P_{78} is not required for SH3 binding but is required for mediating MHC-I down-regulation (Yamada *et al.*, 2003; Casartelli *et al.*, 2006). However, the

mechanism has been unknown. Thus our determination that P_{78} is required for interaction with PACS-1 and PACS-2 explains one role for this site in Nef-induced MHC-I down-regulation (Figure 4). Our results, together with structural studies, suggest, however, that P_{78} does not directly bind the PACS proteins but instead interacts with Y_{120} to stabilize helix αB, enabling W_{113} to interact with the PACS-1 and PACS-2 FBRs (Figures 4–6; Lee *et al.*, 1996; Grzesiek *et al.*, 1997).

Consistent with their failure to interact with PACS proteins, both Nef-E4AP_{78}A and Nef-E4AW_{113}A were mislocalized from the paranuclear region to early or late endosomal compartments (Figures 4 and 7). Strikingly, however, Nef-E4AW_{113}A was frequently observed in varicosities along tubular structures, suggesting the Nef-E4AP_{78}A and Nef-E4AW_{113}A mutants are phenotypically distinct (Figure 7). The extensive tubulation in Nef-E4AW_{113}A–expressing cells was similar to that observed in cells knocked down for retromer-interacting proteins or expressing constitutively active SNX18 (Haberg *et al.*, 2008; Harbour *et al.*, 2010). The colocalization of SNX18 with PACS-1 and AP-1 on endosomes suggests that interaction of PACS proteins with their cargo may modulate vesicle formation and point to how Nef uses PACS-1 and AP-1 to sequester internalized MHC-I (Dikeakos *et al.*, 2010). The extensive tubulation in Nef-E4AW_{113}A–expressing cells may also result from defects in the early endosome recruitment of COPI, which interacts with PACS-2, or disruption of the Rab5/Rab7 switch, perhaps compounded by the intrinsic ability of Nef to induce tubulation (Kottgen *et al.*, 2005; Gerlach *et al.*, 2009; Huotari and Helenius, 2011). These findings suggest new avenues to investigate how membrane trafficking steps regulate Nef action.

The ClusPro 2.0 protein–protein docking server generated a speculative model of the Nef:PACS bipartite binding site that was consistent with the results determined empirically using yeast two-hybrid interaction, in vitro protein binding, and CD spectroscopy (Figure 8). In this model, PACS-1 KR_{185} (KR_{104} in PACS-2) is in the proximity of Nef $EEEE_{65}$ and PACS-1 NK_{189} (NK_{110} in PACS-2) is vicinal to W_{113} in helix αB of the Nef core. Recent benchmarking studies demonstrate that the ClusPro 2.0 server competes with the best human predictor groups to generate reliable receptor:ligand (i.e., Nef:PACS-1) complexes using independently solved structures, provided that there is limited backbone mobility (Kozakov *et al.*, 2010). Thus one caveat of this docking model is location of the $EEEE_{65}$ subsite within the flexible Nef N-terminal region, which can adopt multiple conformations beyond the single fixed receptor conformation used for docking studies. In addition, the structural importance of PACS-1 Q_{195} for binding Nef remains to be determined. Of interest, interaction with furin also requires PACS-1 Q_{195}, albeit not KR_{185}, suggesting this residue is uniquely important for maintaining the distinct cargo-binding subsites in the PACS FBRs defined by Nef and furin (Figure 1 and Supplemental Figure S2; Dikeakos and Thomas, unpublished data). Thus PACS proteins bind at least two subclasses of cargo molecules: proteins like furin that contain CK2 phosphorylatable acidic clusters and those like Nef that contain a bulky hydrophobic residue within an α-helical segment. Because many pathogenic viruses express proteins containing CK2 phosphorylatable acidic cluster motifs that mimic the PACS-binding site in furin and other cellular cargo, we suspect that Nef evolved to bind the adjacent subsite used by as-yet-unidentified cellular proteins (Youker *et al.*, 2009). Together these results illustrate the exquisite cargo selectivity of the PACS proteins. Structural analyses will be required to elucidate the nature of the cargo subsites on the PACS-1 and PACS-2 FBRs with their respective cargoes.

The multiple pathways by which Nef drives HIV-1 disease are achieved in part by the context-specific protein–protein interactions of a limited number of conserved sites in Nef with cellular protein partners (Geyer *et al.*, 2001; Sarmady *et al.*, 2011). For example, in addition to mediating binding to PACS proteins, $EEEE_{65}$ contributes to the ability of Nef to form a complex with AP-1 and the MHC-I cytosolic domain, suggesting that the acidic cluster mediates multiple trafficking steps in the sequestering phase of MHC-I down-regulation (Singh *et al.*, 2009). The $EEEE_{65}$ site is also required for incorporation of Nef into exosomes, for mediating cell-to-cell transfer of Nef through tunneling nanotubes, and for interacting with TRAF2 to promote proinflammatory cytokine signaling (Xu *et al.*, 2009; Ali *et al.*, 2010; Mangino *et al.*, 2011). These findings, together with the location of the $EEEE_{65}$ site in the flexible N-terminal domain, suggest that this site may mediate multiple low-affinity protein–protein interactions that promote high-affinity interactions, such as the interaction between W_{113} in the Nef core and PACS-1 NK_{189}. In this manner, these low- and high-affinity sites may combine to drive the diverse actions of Nef. Within helix αB, L_{112} not only mediates interaction of Nef with PACS-1 and PACS-2, but it also mediates Nef dimerization by combining with Y_{115} to form a hydrophobic surface that stabilizes the interaction between opposite protomers (Poe and Smithgall, 2009). Similarly, whereas W_{113} is required for the interaction of helix αB with PACS-1 and PACS-2, it also combines with F_{90} on helix αA to delimit a hydrophobic pocket that stabilizes the interaction of Nef with SH3 domains (Arold *et al.*, 1997; Poe and Smithgall, 2009; Horenkamp *et al.*, 2011). The determination that the interaction of Nef with PACS-2 or SFKs is mutually exclusive is consistent with the dual role of W_{113} in controlling whether Nef interacts with PACS proteins or with SFKs (Atkins *et al.*, 2008). Whether the W_{113}→A mutation disrupts the Nef–Hck interaction by interfering solely with the PACS-2–dependent trafficking of Nef required for interaction with SFKs or also blocks binding of Nef to the Hck SH3 domain warrants additional studies. It will be important to determine how Nef combines a limited number of binding surfaces to interact with the large set of cellular proteins that enable Nef to drive HIV-1 disease and to use this knowledge to develop new approaches to combat HIV-1.

MATERIALS AND METHODS

Cells, plasmids, virus, and siRNA

HeLa and H9 T cells were cultured as described (Hung *et al.*, 2007; Atkins *et al.*, 2008). To prepare peripheral blood mononuclear cells (PBMCs), peripheral blood was obtained from healthy HLA-A*0201$^+$ volunteers by leukapheresis or by venipuncture using protocols approved by the Oregon Health and Science University Institutional Review Board (protocols IRB00004039 and IRB00002251). Written informed consent was obtained from all subjects according to the Declaration of Helsinki. PBMCs were then cultured in RPMI 1640 containing 10% fetal bovine serum (FBS), nonessential amino acids, and pyruvate and supplemented with IL-2 (50 U/ml; Sigma, St. Louis, MO). Plasmids expressing HA-tagged PACS-1 or PACS-2 or Nef-eYFP were previously described (Hung *et al.*, 2007) and were used to generate site-directed mutations in PACS-1, PACS-2, or Nef mutants using QuikChange Site-Directed Mutagenesis Kit (Agilent Technologies, Santa Clara, CA). Plasmids expressing mcherry-Rab5 or mcherry-Rab7 were provided by T. Weber (Mount Sinai School of Medicine, New York, NY). For the yeast two-hybrid analyses, the Nef, CK2β, and GGA3 sequences were cloned into pBTM116 bait vector, which contains the LexA DNA–binding domain (Liu *et al.*, 1997). The pBTM116 vector expressing furin-DD was described previously (Wan *et al.*, 1998). The PACS sequences were cloned into the pVP16 vector containing the HSV activation domain (Liu *et al.*, 1997). For the protein-binding assays, pGEX-4T PACS-$1_{117\text{-}266}$, and pET3.2a furin-DD were as previously described (Crump *et al.*, 2001;

Simmen *et al.*, 2005). The PACS-$1_{181\text{-}195}$ DNA sequence was synthesized and cloned into pGEX-4T (Celtek Genes, Nashville, TN) and was used to generate PACS-$1_{181\text{-}195}N_{188}A$– and PACS-$1_{181\text{-}195}K_{189}A$–expressing plasmids by QuikChange Mutagenesis. pET-32a His_6-Nef was provided by T. Smithgall (University of Pittsburgh School of Medicine, Pittsburgh, PA) and was used to generate His_6-Nef-E4AW_{113}A using QuikChange Site-Directed Mutagenesis Kit. The ARF1T_{31}N cDNA was provided by T. Roberts (Dana-Farber Cancer Institute, Boston, MA; Addgene [Cambridge, MA] plasmid 10833; Furman *et al*., 2002) and was subcloned into pGEX-4T. For the BiFC analyses, Nef-Yc and a backbone vector containing the amino portion of YFP (Yn) were provided by T. Smithgall. The PACS sequences were inserted 5′ to the Yn fragment by standard cloning techniques. The vaccinia virus recombinant expressing FLAG-tagged Nef (VV:Nef/f) was described previously (Blagoveshchenskaya *et al.*, 2002). The vaccinia virus recombinant expressing FLAG-tagged Nef-EF4AW_{113}A (VV:Nef-EF4AW_{113}A/f) was generated as previously described (Dascher *et al*., 1995). Control (nonspecific) siRNA and siRNAs specific for PACS-2 (Smartpool; Dharmacon, Boulder, CO) were transfected (Lipofectamine 2000; Life Technologies, Grand Island, NY) into cells according to manufacturer's instructions.

Flow cytometry

H9 cells or PBMCs were nucleofected (Amaxa, Gaithersburg, MD) with the plasmids indicated in the figure legends as previously described (Hung *et al.*, 2007). At 40 h postnucleofection, cells were fixed in 2% paraformaldehyde, washed, and resuspended in FACS buffer (phosphate-buffered saline [PBS], pH 7.2, containing 0.5% FBS) and incubated with monoclonal antibody (mAb) BB7.2-PE (anti-HLA-A2; BD Biosciences, San Jose, CA) or mAb W6/32 (anti-MHC-I, 1:4000), followed by PE-conjugated donkey anti–mouse immunoglobulin G (1:500; Jackson ImmunoResearch Laboratories, West Grove, PA) as indicated in the figure legends. Cells were analyzed by listmode acquisition on a FACSCalibur (BD Biosciences) using CellQuest acquisition/analysis software (BD Biosciences), and data were analyzed using CellQuest or FCS express (De Novo Software, Los Angeles, CA).

Coimmunoprecipitation and Western blot

Cells were transfected using Fugene (Roche, Indianapolis, IN) with the indicated plasmids for 48 h and subsequently harvested in PBS containing 1% NP-40, protease inhibitors (0.5 mM phenylmethylsulfonyl fluoride [PMSF] and 0.1 µM aprotinin, E-64, and leupeptin) and phosphatase inhibitors (1 mM Na_3VO_4, 20 mM NaF). HA-tagged PACS constructs were immunoprecipitated with protein G Sepharose (Sigma-Aldrich, St. Louis, MO). The Nef/PACS-1 coimmunoprecipitates were washed in 50 mM Tris (pH 7.4), 175 mM NaCl, and 1% Nonidet P-40, 0.3% deoxycholate, and the Nef/PACS-2 coimmunoprecipitates were washed in 50 mM Tris (pH 7.4), 200 mM NaCl, 1% Nonidet P-40, and 1% deoxycholate. Coimmunoprecipitating proteins were detected by Western blot. The following antibodies were used: anti-His_6 (GenScript, Piscataway, NJ), anti–FLAG mAb M2 (Sigma-Aldrich), anti–HA mAb HA.11 (Covance, San Diego, CA), anti–Nef 2949 (AIDS Research and Reference Reagent Program, National Institutes of Health, Germantown, MD), anti–PACS-1 703 (Atkins *et al*., 2008), anti–PACS-2 193 (Atkins *et al*., 2008), anti–Hck sc-72 (Santa Cruz Biotechnology, Santa Cruz, CA), and anti-actin (Chemicon, Bedford, MA).

Yeast two-hybrid analysis

The L40 yeast strain (MATa his3, trp, ade2, LYS::$(lexAop)_4$-HIS3 URA::$(lexAop)_8$-lacZ GAL4) was cotransformed with a prey plasmid (Leu^- selection) and a bait plasmid (Trp^- selection) as previously described (Liu *et al.*, 1997) and then selected for growth on Leu^-/Trp^- minimal plates. Colonies from the Leu^-/Trp^- plates were streaked onto His^- plates supplemented with 5–50 mM of 3-aminotriazole (3AT) as indicated in the figure legends.

Cell imaging

Cells grown on coverslips were either nucleofected (Nef trafficking experiments) or transfected (BiFC experiments, Lipofectamine 2000) according to the manufacturer's instructions. Samples were washed and fixed immediately with 4% paraformaldehyde or, for BiFC analyses, were preincubated for 3 h at room temperature before fixation. Anti-TfR antibody was provided by C. Enns (Oregon Health and Science University) and was detected using an Alexa Fluor 546 secondary antibody (Life Technologies). Nuclei were stained with 4′,6-diamidino-2-phenylindole (DAPI; Dapi-Fluoromount G; Southern Biotech, Birmingham, AL).

Deconvolution microscopy. Images were acquired on a high-resolution, wide-field Core DeltaVision system (Applied Precision, Issaquah, WA). This system is an Olympus IX71 inverted microscope (Olympus, Center Valley, PA) with a proprietary XYZ stage enclosed in a controlled environment chamber, differential interference contrast transmitted light, and a solid-state module for fluorescence. The camera is a Nikon CoolSNAP ES2 HQ (Nikon, Melville, NY). Each image was acquired as Z- stacks in a 1024 × 1024 or 512 × 512 format with a 60×, 1.42 numerical aperture, PlanApo objective in three colors—YFP, DAPI, and mcherry. The pixel size was 0.107 × 0.107 × 0.4 µm for 512 × 512 × 8 size images and 0.16 × 0.16 × 0.4 µm for 1024 × 1024 × 8 size images. The images were deconvolved with the appropriate optical transfer function using an iterative algorithm of 10 iterations. The histogram was optimized for the most positive image and applied to all the other images for consistency before saving the images as 24-bit merged TIFF files.

Structured illumination microscopy. Images were captured on a Zeiss ELYRA PS.1 system (Carl Zeiss, Jena, Germany). Superresolution images were acquired in three colors with five rotations and reconstructed using Zen 2010 multidimensional software (Gustafsson, 2000). Three-dimensional (3D) image processing was performed using Imaris 7.3.1 (Bitplane, Zurich, Switzerland) to recreate volumes. Surfaces were selected based on the 3D intensity data and represented as pseudocolored images.

Statistical analyses. Statistical analyses for Figures 3C and 4G and the colocalization of Nef-E4AW_{113}A-YFP with endocytic markers in Figure 7A, which are presented in Figure 7B, were compiled using Imaris contour and masking techniques. A precise region of interest (ROI) was selected, and then automated thresholding was used to calculate colocalization statistics. Colocalization was defined as the overlap in the voxels from the red and green channels. The degree of colocalization in each voxel was represented by the percentage of each channel above the threshold and determined to be significant using the unpaired Student's *t* test. Statistics for Figure 3A and the overlap of Rab proteins with Nef-E4AW_{113}A-YFP–containing tubule or donut structures in Figure 7A were compiled using softWoRx Explorer 2.0 (Applied Precision). For the analysis in Figure 3A, a mean intensity reading of the BiFc (YFP) signal was obtained from the cytoplasmic ROI in Nef-Yc–positive cells (identified with anti-Nef 2949 [AIDS Research and Reference Reagent Program], followed by staining

with an Alexa Fluor 546–coupled secondary antibody [Life Technologies]) and from Nef-Yc-negative cells (background). After subtraction of the averaged background signal, the specific BiFC signal was found to be significant using the unpaired Student's *t* test. To determine the association of mcherry-Rab5 or mcherry-Rab7 with Nef-E4AW$_{113}$A-YFP–containing tubule or donut structures in Figure 7A, the structures were first selected in the green (enhanced YFP [eYFP]) channel with the red (mcherry) channel turned off. Nef-E4AW$_{113}$A-eYFP–containing structures were designated as either "tubule" or "donut." The red channel was illuminated, the mcherry-positive spots that associated with each eYFP structure were counted, and the percentage of Nef-E4AW$_{113}$A-eYFP structures (tubule or donut) positive for mcherry-Rab5 or mcherry-Rab7 was determined, with the statistics presented in Figure 7C.

Protein interaction assays

Plasmids expressing GST, GST-PACS-1$_{181\text{-}195}$, GST-PACS-1$_{181\text{-}195}$N$_{188}$A, GST-PACS-1$_{181\text{-}195}$K$_{189}$A, GST-PACS-1$_{117\text{-}266}$, GST-AR-F1T$_{31}$N, His$_6$-Nef, His$_6$-Nef-E4AW$_{113}$A, or His$_6$-furin-DD were transformed in BL21 *Escherichia coli*, and protein expression was induced with 1 mM isopropyl-β-D-thiogalactoside (Calbiochem, Gibbstown, NJ) for 4 h at 37°C. Bacterial pellets were resuspended in lysis buffer (50 mM Tris, pH 7.6, 1.5 mM EDTA, 100 mM NaCl, 0.5% Triton X-100, 0.1 mM dithiothreitol, 10 mM $MgCl_2$) containing protease inhibitors (0.5 mM PMSF and 0.1 μM each of aprotinin, E-64, and leupeptin) and lysed using a French Press (Aminco, Rockville, MD). Soluble material was collected after 1 h of a 25,000 × *g* spin and subsequently bound to glutathione Sepharose 4B (GE Healthcare, Uppsala, Sweden) of Ni^{2+}– nitriloacetic acid (Qiagen, Valencia, CA) for 1 h at 4°C. For the His$_6$-Nef or His$_6$-Furin-DD interaction with GST-PACS the proteins were mixed at a 1:1 ratio for 30 min at 4°C in binding buffer (20 mM Tris, pH 7.9, containing 150 mM NaCl, 0.1 mM EDTA, and 0.1% NP-40). After incubation, glutathione Sepharose 4B was added to the reaction and incubated for an additional 30 min at 4°C. The resin was subsequently washed three times in binding buffer and resuspended in SDS–PAGE sample buffer.

Circular dichroism and protein modeling

Circular dichroism. The 17-mer peptide KRDANKLQIMLQRRKRY (Creative Peptides, Shirley, NY) corresponding to PACS-1$_{184\text{-}200}$ was resuspended in 10 mM potassium phosphate (pH 7.4) at a final concentration of 5 mg/ml. CD spectra were recorded in a Aviv Model 215 spectropolarimeter (Aviv Biomedical, Lakewood, NJ) in a 0.01-cm-thick rectangular quartz cell in a total volume of 30 μλ. In some experiments, the protein denaturant urea or the α-helix stabilizer TFE (Luo and Baldwin, 1997) was added as indicated in the figure legend. Spectra were measured at 0.25-nm intervals from 190- to 260-nm wavelength at 25°C. A background spectrum of buffer alone was measured and used for subtraction from all measured CD spectra. All spectra were averaged from three independent measurements and smoothened by locally weighted polynomial regression. The spectrum in aqueous buffer was fit by a linear combination of the spectra in 3 M urea and 30% TFE using a least-squares algorithm.

Protein modeling. The peptide corresponding to PACS-1$_{181\text{-}195}$ was docked on to the solution structure of Nef (PDB ID: 2Nef) using ClusPro 2.0 (http://cluspro.bu.edu), which automates two steps of protein–protein docking (Grzesiek *et al.*, 1997; Comeau *et al.*, 2004; Kozakov *et al.*, 2010). The first step involves docking of two rigid bodies using a fast Fourier transformation correlation approach that exploits pairwise interaction potentials, and the second step clusters the 1000 best energy conformations, retaining the top 30 largest clusters. ClusPro 2.0 provides the results for docking based on four different coefficients: hydrophobic, electrostatic, balanced, and combined. The balanced coefficient was selected for modeling of Nef:PACS-1$_{181\text{-}95}$ since the PACS-1 structure was based upon ab initio modeling and CD spectroscopy without prior knowledge of the nature of the protein:peptide complex. The subset of docking poses generated using the balanced coefficients are displayed in Figure 5A using surface rendering with 80% transparency (PACS-1$_{181\text{-}95}$) and a ribbon representation (Nef), whereas the model consistent with the experimental data is depicted as a ribbon in Figure 8A. All structures were visualized using PyMOL (www.pymol.org).

ACKNOWLEDGMENTS

We thank T. Smithgall, T. Weber, T. Roberts, C. D. Hu, and C. Enns for reagents and T. Dillon, T. Smithgall, and L. L. Thomas for critically reading the manuscript. We thank A. Snyder of the Jungers Center Advanced Light Microscopy Core (Oregon Health and Science University) and K. M. Atkins, L. L. Thomas, and L. Larsen for experimental assistance. This work was supported by Canadian Institutes of Health Research Fellowship HFE-87760, Fonds de recherche du Québec-Santé Fellowship 23037, the Collins Medical Trust (J.D.D.), National Science Foundation Grant MCB0746589 and the American Heart Association (U.S.), National Institutes of Health Grants S10-RR023432 (to the Advanced Light Microscopy Core), and DK37274 and CA151564 (G.T.).

REFERENCES

Ali SA, Huang MB, Campbell PE, Roth WW, Campbell T, Khan M, Newman G, Villinger F, Powell MD, Bond VC (2010). Genetic characterization of HIV type 1 Nef-induced vesicle secretion. AIDS Res Hum Retroviruses 26, 173–192.

Arold S, Franken P, Strub MP, Hoh F, Benichou S, Benarous R, Dumas C (1997). The crystal structure of HIV-1 Nef protein bound to the Fyn kinase SH3 domain suggests a role for this complex in altered T cell receptor signaling. Structure 5, 1361–1372.

Aslan JE *et al.* (2009). Akt and 14-3-3 control a PACS-2 homeostatic switch that integrates membrane traffic with TRAIL-induced apoptosis. Mol Cell 34, 497–509.

Atkins KM, Thomas L, Youker RT, Harriff MJ, Pissani F, You H, Thomas G (2008). HIV-1 Nef binds PACS-2 to assemble a multikinase cascade that triggers major histocompatibility complex class I (MHC-I) down-regulation: analysis using short interfering RNA and knock-out mice. J Biol Chem 283, 11772–11784.

Blagoveshchenskaya AD, Thomas L, Feliciangeli SF, Hung CH, Thomas G (2002). HIV-1 Nef down-regulates MHC-I by a PACS-1- and PI3K-regulated ARF6 endocytic pathway. Cell 111, 853–866.

Bouard D, Sandrin V, Boson B, Negre D, Thomas G, Granier C, Cosset FL (2007). An acidic cluster of the cytoplasmic tail of the RD114 virus glycoprotein controls assembly of retroviral envelopes. Traffic 8, 835–847.

Casartelli N, Giolo G, Neri F, Haller C, Potesta M, Rossi P, Fackler OT, Doria M (2006). The Pro78 residue regulates the capacity of the human immunodeficiency virus type 1 Nef protein to inhibit recycling of major histocompatibility complex class I molecules in an SH3-independent manner. J Gen Virol 87, 2291–2296.

Chen J, Wang J, Meyers KR, Enns CA (2009). Transferrin-directed internalization and cycling of transferrin receptor 2. Traffic 10, 1488–1501.

Comeau SR, Gatchell DW, Vajda S, Camacho CJ (2004). ClusPro: a fully automated algorithm for protein-protein docking. Nucleic Acids Res 32, W96–W99.

Crump CM, Hung CH, Thomas L, Wan L, Thomas G (2003). Role of PACS-1 in trafficking of human cytomegalovirus glycoprotein B and virus production. J Virol 77, 11105–11113.

Crump CM, Xiang Y, Thomas L, Gu F, Austin C, Tooze SA, Thomas G (2001). PACS-1 binding to adaptors is required for acidic cluster motif-mediated protein traffic. EMBO J 20, 2191–2201.

Dascher C, VanSlyke JK, Thomas L, Balch WE, Thomas G (1995). Preparation of recombinant vaccinia virus for expression of small GTPases. Methods Enzymol 257, 174–188.
Dikeakos JD *et al.* (2010). Small molecule inhibition of HIV-1-induced MHC-I down-regulation identifies a temporally regulated switch in Nef action. Mol Biol Cell 21, 3279–3292.
Fackler OT, Baur AS (2002). Live and let die: Nef functions beyond HIV replication. Immunity 16, 493–497.
Faure J, Stalder R, Borel C, Sobo K, Piguet V, Demaurex N, Gruenberg J, Trono D (2004). ARF1 regulates Nef-induced CD4 degradation. Curr Biol 14, 1056–1064.
Friedrich TC *et al.* (2004). Reversion of CTL escape-variant immunodeficiency viruses in vivo. Nat Med 10, 275–281.
Friedrich TC *et al.* (2010). High viremia is associated with high levels of in vivo major histocompatibility complex class I down-regulation in rhesus macaques infected with simian immunodeficiency virus SIVmac239. J Virol 84, 5443–5447.
Furman C, Short SM, Subramanian RR, Zetter BR, Roberts TM (2002). DEF-1/ASAP1 is a GTPase-activating protein (GAP) for ARF1 that enhances cell motility through a GAP-dependent mechanism. J Biol Chem 277, 7962–7969.
Geijtenbeek TB, Gringhuis SI (2009). Signalling through C-type lectin receptors: shaping immune responses. Nat Rev Immunol 9, 465–479.
Gerlach H, Laumann V, Martens S, Becker CF, Goody RS, Geyer M (2009). HIV-1 Nef membrane association depends on charge, curvature, composition and sequence. Nat Chem Biol 6, 46–53.
Geyer M, Fackler OT, Peterlin BM (2001). Structure–function relationships in HIV-1 Nef. EMBO Rep 2, 580–585.
Greenberg ME, Iafrate AJ, Skowronski J (1998). The SH3 domain-binding surface and an acidic motif in HIV-1 Nef regulate trafficking of class I MHC complexes. EMBO J 17, 2777–2789.
Grzesiek S, Bax A, Hu JS, Kaufman J, Palmer I, Stahl SJ, Tjandra N, Wingfield PT (1997). Refined solution structure and backbone dynamics of HIV-1 Nef. Protein Sci 6, 1248–1263.
Guruprasad K, Reddy BV, Pandit MW (1990). Correlation between stability of a protein and its dipeptide composition: a novel approach for predicting in vivo stability of a protein from its primary sequence. Protein Eng 4, 155–161.
Gustafsson MG (2000). Surpassing the lateral resolution limit by a factor of two using structured illumination microscopy. J Microsc 198, 82–87.
Haberg K, Lundmark R, Carlsson SR (2008). SNX18 is an SNX9 paralog that acts as a membrane tubulator in AP-1-positive endosomal trafficking. J Cell Sci 121, 1495–1505.
Harbour ME, Breusegem SY, Antrobus R, Freeman C, Reid E, Seaman MN (2010). The cargo-selective retromer complex is a recruiting hub for protein complexes that regulate endosomal tubule dynamics. J Cell Sci 123, 3703–3717.
Horenkamp FA, Breuer S, Schulte A, Lulf S, Weyand M, Saksela K, Geyer M (2011). Conformation of the dileucine-based sorting motif in HIV-1 Nef revealed by intermolecular domain assembly. Traffic 12, 867–877.
Hung CH *et al.* (2007). HIV-1 Nef assembles a Src family kinase-ZAP-70/Syk-PI3K cascade to down-regulate cell-surface MHC-I. Cell Host Microbe 1, 121–133.
Huotari J, Helenius A (2011). Endosome maturation. EMBO J 30, 3481–3500.
Jenkins PM, Zhang L, Thomas G, Martens JR (2009). PACS-1 mediates phosphorylation-dependent ciliary trafficking of the cyclic-nucleotide-gated channel in olfactory sensory neurons. J Neurosci 29, 10541–10551.
Kerppola TK (2008). Bimolecular fluorescence complementation (BiFC) analysis as a probe of protein interactions in living cells. Annu Rev Biophys 37, 465–487.
Kirchhoff F (2010). Immune evasion and counteraction of restriction factors by HIV-1 and other primate lentiviruses. Cell Host Microbe 8, 55–67.
Kirchhoff F, Easterbrook PJ, Douglas N, Troop M, Greenough TC, Weber J, Carl S, Sullivan JL, Daniels RS (1999). Sequence variations in human immunodeficiency virus type 1 Nef are associated with different stages of disease. J Virol 73, 5497–5508.
Kottgen M *et al.* (2005). Trafficking of TRPP2 by PACS proteins represents a novel mechanism of ion channel regulation. EMBO J 24, 705–716.
Kozakov D *et al.* (2010). Achieving reliability and high accuracy in automated protein docking: ClusPro, PIPER, SDU, and stability analysis in CAPRI rounds 13-19. Proteins 78, 3124–3130.
Lee CH, Saksela K, Mirza UA, Chait BT, Kuriyan J (1996). Crystal structure of the conserved core of HIV-1 Nef complexed with a Src family SH3 domain. Cell 85, 931–942.
Lieberman J (2003). The ABCs of granule-mediated cytotoxicity: new weapons in the arsenal. Nat Rev Immunol 3, 361–370.
Liu G, Thomas L, Warren RA, Enns CA, Cunningham CC, Hartwig JH, Thomas G (1997). Cytoskeletal protein ABP-280 directs the intracellular trafficking of furin and modulates proprotein processing in the endocytic pathway. J Cell Biol 139, 1719–1733.
Luo P, Baldwin RL (1997). Mechanism of helix induction by trifluoroethanol: a framework for extrapolating the helix-forming properties of peptides from trifluoroethanol/water mixtures back to water. Biochemistry 36, 8413–8421.
Mangino G *et al.* (2011). HIV-1 Nef induces proinflammatory state in macrophages through its acidic cluster domain: involvement of TNF alpha receptor associated factor 2. PLoS One 6, e22982.
McMichael AJ, Borrow P, Tomaras GD, Goonetilleke N, Haynes BF (2010). The immune response during acute HIV-1 infection: clues for vaccine development. Nat Rev Immunol 10, 11–23.
Molloy SS, Thomas L, Kamibayashi C, Mumby MC, Thomas G (1998). Regulation of endosome sorting by a specific PP2A isoform. J Cell Biol 142, 1399–1411.
Myhill N, Lynes EM, Nanji JA, Blagoveshchenskaya AD, Fei H, Simmen KC, Cooper TJ, Thomas G, Simmen T (2008). The subcellular distribution of calnexin is mediated by PACS-2. Mol Biol Cell 19, 2777–2788.
Noviello CM, Benichou S, Guatelli JC (2008). Cooperative binding of the class I major histocompatibility complex cytoplasmic domain and human immunodeficiency virus type 1 Nef to the endosomal AP-1 complex via its mu subunit. J Virol 82, 1249–1258.
Peterlin BM, Trono D (2003). Hide, shield and strike back: how HIV-infected cells avoid immune eradication. Nat Rev Immunol 3, 97–107.
Piguet V, Wan L, Borel C, Mangasarian A, Demaurex N, Thomas G, Trono D (2000). HIV-1 Nef protein binds to the cellular protein PACS-1 to down-regulate class I major histocompatibility complexes. Nat Cell Biol 2, 163–167.
Poe JA, Smithgall TE (2009). HIV-1 Nef dimerization is required for Nef-mediated receptor down-regulation and viral replication. J Mol Biol 394, 329–342.
Roeth JF, Williams M, Kasper MR, Filzen TM, Collins KL (2004). HIV-1 Nef disrupts MHC-I trafficking by recruiting AP-1 to the MHC-I cytoplasmic tail. J Cell Biol 167, 903–913.
Sarmady M, Dampier W, Tozeren A (2011). HIV protein sequence hotspots for crosstalk with host hub proteins. PLoS One 6, e23293.
Schaefer MR, Wonderlich ER, Roeth JF, Leonard JA, Collins KL (2008). HIV-1 Nef targets MHC-I and CD4 for degradation via a final common beta-COP-dependent pathway in T cells. PLoS Pathog 4, e1000131.
Schermer B *et al.* (2005). Phosphorylation by casein kinase 2 induces PACS-1 binding of nephrocystin and targeting to cilia. EMBO J 24, 4415–4424.
Scott GK, Fei H, Thomas L, Medigeshi GR, Thomas G (2006). A PACS-1, GGA3 and CK2 complex regulates CI-MPR trafficking. EMBO J 25, 4423–4435.
Sieburth D *et al.* (2005). Systematic analysis of genes required for synapse structure and function. Nature 436, 510–517.
Simmen T, Aslan JE, Blagoveshchenskaya AD, Thomas L, Wan L, Xiang Y, Feliciangeli SF, Hung CH, Crump CM, Thomas G (2005). PACS-2 controls endoplasmic reticulum-mitochondria communication and Bid-mediated apoptosis. EMBO J 24, 717–729.
Singh RK, Lau D, Noviello CM, Ghosh P, Guatelli JC (2009). An MHC-I cytoplasmic domain/HIV-1 Nef fusion protein binds directly to the mu subunit of the AP-1 endosomal coat complex. PLoS One 4, e8364.
Wan L, Molloy SS, Thomas L, Liu G, Xiang Y, Rybak SL, Thomas G (1998). PACS-1 defines a novel gene family of cytosolic sorting proteins required for *trans*-Golgi network localization. Cell 94, 205–216.
Xu W *et al.* (2009). HIV-1 evades virus-specific IgG2 and IgA responses by targeting systemic and intestinal B cells via long-range intercellular conduits. Nat Immunol 10, 1008–1017.
Yamada T, Kaji N, Odawara T, Chiba J, Iwamoto A, Kitamura Y (2003). Proline 78 is crucial for human immunodeficiency virus type 1 Nef to down-regulate class I human leukocyte antigen. J Virol 77, 1589–1594.
Youker RT, Shinde U, Day R, Thomas G (2009). At the crossroads of homoeostasis and disease: roles of the PACS proteins in membrane traffic and apoptosis. Biochem J 421, 1–15.